AGU PUBLICATIONS

JGR

Journal of Geophysical Research: Planets

RESEARCH ARTICLE
10.1002/2016JE005195

Key Points:
- Curiosity obtained bulk chemistry for sedimentary rocks in the Bradbury group
- Coarse-grained rocks are enriched in plagioclase
- Geochemical trends are consistent with mineral sorting during transport

Supporting Information:
- Supporting Information S1
- Table S1

Correspondence to:
K. L. Siebach,
kirsten.siebach@stonybrook.edu

Citation:
Siebach, K. L., M. B. Baker, J. P. Grotzinger, S. M. McLennan, R. Gellert, L. M. Thompson, and J. A. Hurowitz (2017), Sorting out compositional trends in sedimentary rocks of the Bradbury group (Aeolis Palus), Gale crater, Mars, *J. Geophys. Res. Planets*, *122*, 295–328, doi:10.1002/2016JE005195.

Received 10 OCT 2016
Accepted 1 JAN 2017
Accepted article online 5 JAN 2017
Published online 2 FEB 2017

Sorting out compositional trends in sedimentary rocks of the Bradbury group (Aeolis Palus), Gale crater, Mars

K. L. Siebach[1,2], M. B. Baker[1], J. P. Grotzinger[1], S. M. McLennan[2], R. Gellert[3], L. M. Thompson[4], and J. A. Hurowitz[2]

[1]Division of Geological and Planetary Sciences, California Institute of Technology, Pasadena, California, USA, [2]Department of Geosciences, SUNY at Stony Brook, Stony Brook, New York, USA, [3]Department of Physics, University of Guelph, Guelph, Ontario, Canada, [4]Planetary and Space Science Centre, University of New Brunswick, Fredericton, New Brunswick, Canada

Abstract Sedimentary rocks are composed of detrital grains derived from source rocks, which are altered by chemical weathering, sorted during transport, and cemented during diagenesis. Fluvio-lacustrine sedimentary rocks of the Bradbury group, observed on the floor of Gale crater by the Curiosity rover during its first 860 Martian solar days, show trends in bulk chemistry that are consistent with sorting of mineral grains during transport. The Bradbury group rocks are uniquely suited for sedimentary provenance analysis because they appear to have experienced negligible cation loss (i.e., open-system chemical weathering) at the scale of the Alpha Particle X-ray Spectrometer bulk chemistry analyses based on low Chemical Index of Alteration values and successful modeling of >90% of the (volatile-free) targets as mixtures of primary igneous minerals. Significant compositional variability between targets is instead correlated to grain-size and textural characteristics of the rocks; the coarsest-grained targets are enriched in Al_2O_3, SiO_2, and Na_2O, whereas the finer-grained targets are enriched in mafic components. This is consistent with geochemical and mineralogical modeling of the segregation of coarse-grained plagioclase from finer-grained mafic minerals (e.g., olivine and pyroxenes), which would be expected from hydrodynamic sorting of the detritus from mechanical breakdown of subalkaline plagioclase-phyric basalts. While the presence of a distinctive K_2O-rich stratigraphic interval shows that input from at least one distinctive alkali-feldspar-rich protolith contributed to basin fill, the dominant compositional trends in the Bradbury group are consistent with sorting of detrital minerals during transport from relatively homogeneous plagioclase-phyric basalts.

1. Introduction

Sedimentary rocks are repositories for detrital grains derived from all rock types present in their source regions. This detrital material is altered by weathering, sorted by transport processes, and cemented by diagenetic fluids. The Mars Science Laboratory rover, *Curiosity*, has shown that Gale crater contains significant volumes of sedimentary rock, creating both the modern floor of the crater (Aeolis Palus) and the 5 km tall stack of sedimentary rock in the middle of the crater that makes up Mount Sharp (Aeolis Mons) [*Grotzinger et al*., 2015]. As of Martian solar day (sol) 860, *Curiosity* had traversed across 9.5 km of the crater floor and observed over 65 m of stratigraphy dominated by lithified fluvial deposits known as the Bradbury group [*Grotzinger et al*., 2015]. These sedimentary deposits are invaluable tools for understanding the nature and variety of rock types in the Noachian-era terrain that makes up the region around Gale crater and which was eroded to produce the material that filled the crater basin. However, deriving provenance information from bulk compositions of sedimentary rocks requires accounting for weathering, transport, alteration, and cementation processes that can modify sedimentary rock compositions relative to their sources.

The bulk compositions of sedimentary rocks are significantly simpler to relate to the compositions of their source rocks if no open-system chemical alteration—i.e., changes in the bulk chemistry related to preferential leaching or retention of select elements—has occurred due to initial weathering of bedrock source regions or due to later diagenesis during sediment burial. A useful tool for measuring the extent of open-system chemical weathering using compositional data for terrestrial and/or Martian sediments is the Chemical Index of Alteration (CIA), a ratio of Al_2O_3 to labile cations (Ca, Na, and K) designed as a chemical proxy for the degree of alteration of feldspars and, in the case of mafic rocks, Ca-bearing pyroxene [*Nesbitt and Young*, 1982, 1984;

McLennan et al., 2014]. CIA values for Aeolis Palus (i.e., Bradbury group rocks) are uniformly low, typically below 40 and always below 45, beneath even those values associated with incipient weathering of terrestrial basalts, strongly suggesting that chemical alteration of these sediments has been cation conservative at the scale of the bulk chemistry measurements by the Alpha Particle X-ray Spectrometer (centimeter scale) [e.g., *McLennan et al*., 2014]. We thus proceed with the simplest interpretation of the CIA data—that there was no significant open-system weathering of the Bradbury group sediments. Assumptions inherent to this model are discussed further in section 5.

In the assumed absence of open-system chemical weathering, there are three significant factors that control the composition of sedimentary rocks: (1) the source rocks in the watershed, (2) erosion and transport processes that sort detrital and mineral grains by size and density [*McGlynn et al*., 2012; *Fedo et al*., 2015], and (3) addition of diagenetic cements [*McLennan et al*., 2003; *Nesbitt*, 2003]. Each of these factors must be considered when interpreting the compositional variations in a set of sedimentary rocks.

1. The source rocks contributing to a watershed vary with space and time. Erosion is not uniform in space or time, and this can cause variations in the proportional contributions of different exposed rock units and/or exposure of new rock units. For the Bradbury group, this problem is made tractable by (a) uniformly low CIA values, which indicate that all or the large majority of contributing source rocks are basaltic rocks, and so, as igneous rocks, their compositions and minerals reflect the constraints of phase equilibria [*Nesbitt and Young*, 1982, 1996], and (b) measurements of the compositions of Bradbury group rocks at different stratigraphic heights, which allow the ebb and flow of distinctive units to be traced, providing some constraint on changes in sedimentary input as a function of time [e.g., *Nesbitt and Young*, 1982; *Fedo et al*., 1997].
2. Rock breakdown [*Fedo et al*., 2015] and transport [*Frihy et al*., 1995; *Ferguson et al*., 1996; *Nesbitt and Young*, 1996; *Komar*, 2007; *Mangold et al*., 2011] processes have long been known to sort minerals and lithic fragments by size and density [*Mackie*, 1923]. Initial erosion/breakdown tends to isolate phenocryst minerals and can segregate other minerals based on erodibility [*Nesbitt and Young*, 1996; *Fedo et al*., 2015]. Transport processes further sort both mineral grains and lithic fragments by density and size, sometimes well enough to create heavy mineral placers of economic significance [*Frihy et al*., 1995; *Hughes et al*., 2000]. These processes strongly affect the relationship between the sedimentary rock compositions and the source rock compositions and can be assessed by comparison of the sedimentary rock compositions with their grain sizes and depositional environments.
3. Lithification of sedimentary rock typically involves physical compaction and chemical cementation by oversaturated groundwater fluids that interact with the sediments after they are deposited and precipitate minerals in the intergranular void spaces [*Worden and Burley*, 2003]. Compaction alone does not change rock composition, but interactions with cementing groundwater fluids can alter the initial sediment composition by cement addition or by chemical alteration (dissolution and leaching of the detrital mineral grains). Cementation is assured for Bradbury rocks owing to their high degree of lithification and small amounts of residual porosity. However, for many of these rocks, cement compositions are poorly constrained—an issue that we return to in section 5.

More than 100 measurements of the bulk compositions of outcrop and float rocks within Aeolis Palus, taken by the Alpha Particle X-ray Spectrometer (APXS) instrument on board *Curiosity* between sols 0 and 860, provide a compositional data set spanning a significant range of sedimentary rock textures. This study aims to use the compositions of the rocks observed by *Curiosity* to constrain the influence of each of the factors discussed above, with implications for the range of contributing basaltic provenances and the extent of aqueous diagenesis.

2. Geologic Context

Gale crater is a 155 km diameter crater sitting on fluvially dissected Noachian terrain on the Martian topographical dichotomy boundary. Crater counts of the Gale crater ejecta blanket indicate that the impact occurred 3.8–3.6 Gyr. Perhaps the most dominant feature of Gale crater is the 5 km thick stack of sediments forming the crescent-shaped Mount Sharp (Aeolis Mons) in the center of the crater [*Malin and Edgett*, 2000]. This stack of sediments includes layers that were correlated with phyllosilicate and

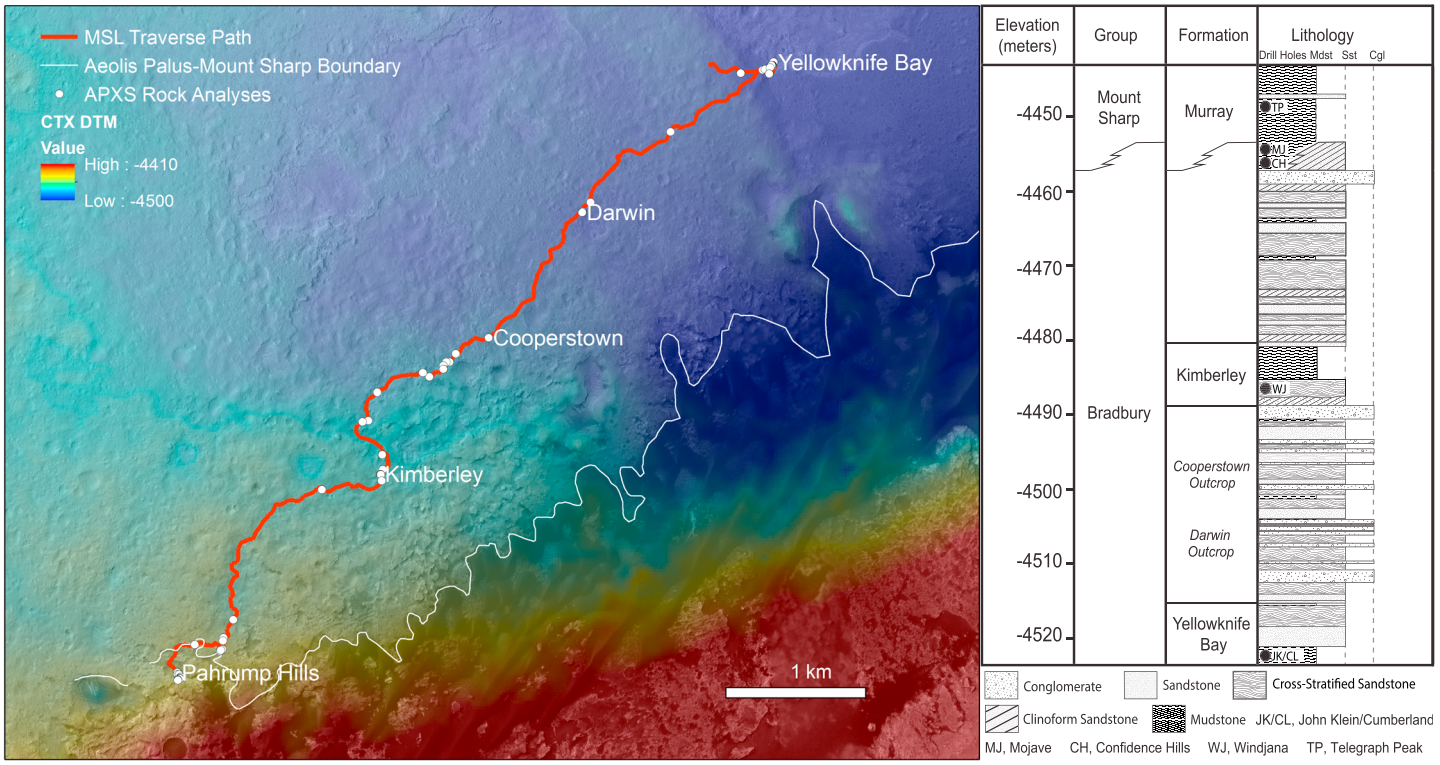

Figure 1. Overhead map showing the location and climbing elevation of the 9.5 km traverse path of the *Curiosity* rover during the first 860 sols after landing, with the stratigraphic column over the same portion of the traverse (based on elevation) on the right [*Grotzinger et al.*, 2015]. Major outcrops labeled. Rover traverse begins west of Yellowknife Bay, jogs east to Yellowknife Bay, and then continues to the southwest. Locations of APXS analyses are marked with white dots. White line on map represents the main transition from Aeolis Palus (Bradbury group) rocks to Mount Sharp group rocks at the Pahrump Hills outcrop, reached on sol 750, although these facies are interfingered as shown in stratigraphic column.

sulfate mineral detections in orbital spectroscopy data sets and motivated the selection of Gale crater as the landing site for the *Curiosity* rover [*Anderson and Bell*, 2010; *Milliken et al.*, 2010].

Comparisons between Gale and other complex craters of similar size indicate that Mount Sharp is constructed around a tall central peak and the modern floor of Gale crater is likely underlain by 1–2 km of sedimentary rock [*Grotzinger et al.*, 2015]. This and other work with infilled craters suggest that much of the crater was once filled with sediments, and the current topography is based on eolian erosion of a "moat" around the central peak/Mount Sharp complex [*Malin and Edgett*, 2000; *Farley et al.*, 2014; *Grotzinger et al.*, 2015]. This hypothesis implies that sedimentary rocks in the moat (i.e., the Bradbury group in Aeolis Palus) may be genetically related to the lowest exposed layers in Mount Sharp [*Grotzinger et al.*, 2015].

The *Curiosity* rover landed at Bradbury Rise, a topographic high within Aeolis Palus about 9 km from the geologic contact between the Bradbury group and the Murray formation (Figure 1) and explored ~61 m of the Bradbury group stratigraphy. Rocks interpreted to be lacustrine mudstones were analyzed at the base of the stratigraphic section at Yellowknife Bay and also in the Murray formation at Pahrump Hills. The bulk of the intervening Bradbury group comprises a series of pebbly sandstones, conglomerates, and siltstone sedimentary rocks of fluvio-deltaic origin (Figure 1) [*Grotzinger et al.*, 2015]. While some large clasts within conglomerates and some float rocks are potentially igneous in composition, the observed stratigraphic sequence of in-place rocks in Aeolis Palus is composed exclusively of sedimentary rocks. All measured beds within this portion of the traverse are approximately horizontal, so we will assume that elevation is a good proxy for stratigraphic position within these units [*Grotzinger et al.*, 2014; *Grotzinger et al.*, 2015].

3. Methods

3.1. APXS

The Alpha-Particle X-ray Spectrometer (APXS) instrument mounted on *Curiosity*'s robotic arm enables in situ X-ray spectroscopy, providing the average composition of a target within a 1.5 cm diameter circle [*Gellert et al*., 2009; *Campbell et al*., 2012; *Gellert and Clark*, 2015]. Regularly reported oxides and trace elements are (wt %) Na_2O; MgO; Al_2O_3; SiO_2; P_2O_5; SO_3; Cl; K_2O; CaO; TiO_2; Cr_2O_3; MnO; FeO_T; and (ppm) Ni, Zn, and Br. Note that APXS provides no information concerning the oxidation states of Fe and S; concentrations of these two elements are simply reported as FeO_T (all Fe as FeO) and SO_3, respectively. Details concerning the APXS instrument, data reduction, and precision are given in Appendix A1.

Within the Bradbury group, 112 APXS analyses were collected on or offset from (i.e., partially overlapping) 73 named targets. For this study, all analyses were included except for repeated analyses of the same surface in the same location, for which only the measurement with the longest integration time was included. For geochemical models described in sections 4.2 and 4.4, compositions were used "as reported" (i.e., normalized to 100 wt % with SO_3 and Cl); for the mineralogical modeling discussed in section 4.6, bulk compositions were normalized on a SO_3- and Cl-free basis. More details on how we treated multiple analyses on the same rock and a justification for using volatile-free bulk compositions in the mass balance models are available in Appendix A1.

3.2. Mars Hand Lens Imager

The Mars Hand Lens Imager (MAHLI) instrument is a high-resolution focusing color camera mounted on *Curiosity*'s robotic arm. It can focus at distances between ~2.1 cm and infinity and is typically used for high-resolution (14+ μm/pixel) imaging of targets of interest, including all APXS targets [*Edgett et al*., 2012]. For this study, the MAHLI images taken with ~5 cm standoff distance (~30 μm/pixel) for each of the APXS targets were used for initial textural comparison, and the specific image numbers used are listed in Table S1 in the supporting information (images are available through the NASA Planetary Data System). In the few cases where such imagery was not taken, higher standoff distances or images from the Mastcam were used to determine textures. For some targets, higher-resolution imagery is also available, and this was used whenever possible to clarify grain sizes and compare textures.

4. Results

4.1. Rock Classification by Texture

The classification of detrital sedimentary rocks is typically based on the sizes of the grains within the rock. On Mars, grain-size assessment can be complicated for several reasons: first, the MAHLI resolution limit at a typical standoff distance is ~30 μm/pixel, so only grains larger than ~50–100 μm are distinguishable; second, the in situ rock surfaces are commonly dust covered, obscuring grain boundaries; and third, many of the targets *Curiosity* has observed have extremely homogeneous coloring, making it even more difficult to clearly distinguish grains from cement or matrix. Other classification schemes in the literature use texture, chemical composition, and inferred igneous or sedimentary origin to define rock classes [e.g., *Mangold et al*., 2017]. For the collection of rock surface targets that Mars Science Laboratory (MSL) analyzed with APXS and MAHLI in the first 860 sols, the classification system defined here is based on texture alone, using grain size wherever possible and surface texture and coloring when grain sizes could not be distinguished. Although texturally similar, the Murray mudstone formation in the Mount Sharp group was separated from the Bradbury group mudstones due to its distinctive stratigraphic context. Targets with clear diagenetic overprinting (e.g., nodular and dendritic concretions and fracture fills [e.g., *Nachon et al*., 2014; *Siebach et al*., 2014; *Stack et al*., 2014; *VanBommel et al*., 2016]) were further split into their own category. Analyses of soils and rock powders produced by drilling were excluded from this analysis; only rock surface targets were considered. Float rocks were included since they may be related to the Bradbury group, although they lack stratigraphic context and could also be unrelated and/or potentially moved by impact processes. In total, eight classes (seven textural classes in the Bradbury group and one class from the Mount Sharp group) were identified to encompass the range of MAHLI and APXS rock surface targets observed by *Curiosity* in the first 860 sols: Sheepbed mudstone (Figure 2a), fine sandstone (Figure 2b), sandstone (Figure 2c), conglomerate (Figure 2d), uncertain

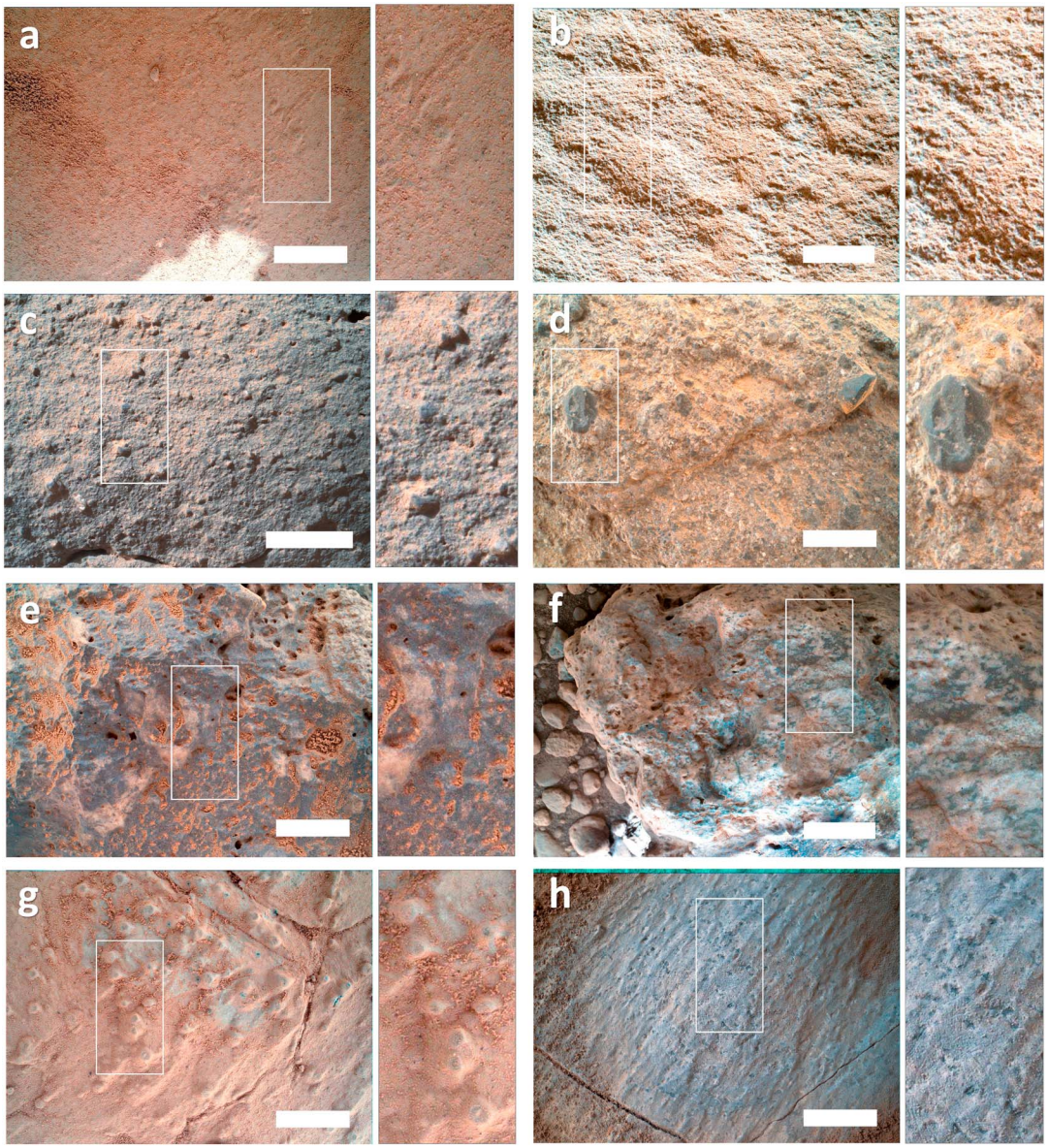

Figure 2. (a–g) MAHLI image examples of each of the textural classes of rocks in the Bradbury group and (h) the Murray mudstone in the Mount Sharp group. White scale bars are 1 cm across. Classes were divided on the basis of grain size and/or surface texture and coloring and include (Figure 2a) Sheepbed mudstone (10 APXS analyses; example is Wernecke_preDRT, sol 168), exposed in Yellowknife Bay with grains finer than the limit of resolution; (Figure 2b) fine sandstone (15 APXS analyses; example is Aillik1, sol 322), well-sorted siltstones to sandstones; (Figure 2c) sandstone (22 APXS analyses; example is Gillespie_Lake, sol 132), medium to pebbly sandstones; (Figure 2d) conglomerate (15 APXS analyses; example is Bardin_Bluffs, sol 394), primary grain sizes >1 mm, rounded grains, clasts up to 6 cm; (Figure 2e) uncertain (13 APXS analyses; example is Morehouse, sol 503), float rocks with poorly defined grain boundaries, sometimes weather like conglomerates; (Figure 2f) possible igneous (4 APXS analyses; example is Clinton, sol 512), small group of float rocks and one clast in a conglomerate with porphyritic textures, shortened to "igneous" in plot legends; (Figure 2g) diagenetic (36 APXS analyses; example is CumberlandNewRP_LIBs, sol 277), rocks with clearly diagenetic textures including preferential cementation and fracture fills; and (Figure 2h) Murray mudstone (27 APXS analyses; example is Punchbowl2, sol 813), mudstone observed at Pahrump Hills in Mount Sharp group, fine grained with potential secondary crystal structures. MAHLI image IDs are in Table S1.

(Figure 2e), possible igneous (Figure 2f), diagenetic (Figure 2g), and Murray mudstone (Figure 2h). Each of these textural classes is described in detail below:

Sheepbed mudstone (10 analyses; Figure 2a) The Sheepbed mudstone member is the lowermost stratigraphic unit of the Yellowknife Bay formation, described in detail in *Grotzinger et al.* [2014]. The rock texture in this unit was extremely smooth at the MAHLI resolution (up to 15 μm/pixel). There were a variety of diagenetic targets within this unit (20 analyses) where we examined concretions, raised ridge features, and/or light-toned veins, which were categorized as diagenetic targets and excluded from the Sheepbed mudstone

category. Several of the analyses in this category were on dusty surfaces. The Sheepbed formation name is included in the textural classification because no mudstones outside of this unit were observed within the Bradbury group.

Fine sandstone (15 analyses; Figure 2b) The fine sandstone category includes analyses of sandstones or siltstones with grain sizes approximately at the MAHLI limit of resolution. These are all well-sorted siltstones to fine sandstones and do not have visible grains larger than ~200 μm.

Sandstone (22 analyses; Figure 2c) The sandstone category includes analyses of medium-grained, sometimes pebbly (e.g., clinoform sandstones in *Grotzinger et al*. [2015]), sandstones that are primarily composed of $<$0.5 mm grains. These grains (exclusive of sparse pebbles) range from well sorted to poorly sorted. Void space mapping on these targets indicated that apparent primary porosity is quite low, so these rocks were well cemented, although the cement composition is unknown. Visible secondary porosity is rare and potentially reflects relatively modern surface weathering [*Siebach and Grotzinger*, 2014]. Where pebbly, clasts range up to a centimeter in diameter and are dispersed in the sandstone matrix.

Conglomerate (15 analyses; Figure 2d) Conglomerate targets include those rocks with primary grain sizes $>$1 mm (coarse sandstones and conglomerates on the Wentworth scale [*Wentworth*, 1922]). These are typically poorly sorted and show variable cementation, both within a given outcrop and across the traverse. Some of these targets have significant dust cover. Individual clasts, where identifiable and not dusty, range from light toned to dark toned and from subangular to subrounded. The largest clasts are up to 6 cm across on the longest axis. End-members of this class range from variably cemented rocks with clearly identifiable grains (e.g., Mount Bastion, sol 399; and Bardin Bluffs, sol 394) to well-cemented conglomerates that are more homogeneous in color but have a vuggy surface texture from weathering that reveals clast boundaries (e.g., Oneida, sol 506; and JumJum, sol 550).

Uncertain (13 analyses; Figure 2e) The uncertain category contains a subset of float rocks whose dust cover and weathering textures make it difficult to define any grain boundaries, indicating that either the grains are below the resolution limit of the image or that they are well cemented and relatively homogeneous in color. A number of rocks in this category have some weathering textures or color changes that hint at the presence of larger grains, but these grains are not well defined. Some of these rocks look very similar to the well-cemented conglomerates with homogeneous surface color, but they are assigned to this category because the grain boundaries are not defined and their context is unknown because they are float rocks (e.g., Nedrow, sol 503; Kodak, sol 512; and Monkey Yard, sol 564). Other rocks in this category show some variability in color, including light-toned patches several millimeters in size that blend back into the dark gray rock, but the colors blend together instead of creating sharp grain boundaries (e.g., Morehouse, sol 503; and Lowerre and Larrabee, sol 510). Finally, a few rocks in this category do not show any clear evidence for visible grains and may be quite fine grained. These tend to exhibit a vuggy texture that further obfuscates their origin. Some of these have been categorized by other authors in dramatically different ways, for example, as fine-grained igneous rocks or alternatively as iron-oxide-cemented, fine-grained sedimentary rocks (e.g., Jake Matijevic, sols 46 and 47; Et Then, sols 86 and 90; and Secure, sol 560) [*Stolper et al*., 2013; *Blaney et al*., 2014], and accordingly, some caution is warranted in discussing these rocks.

Possible igneous (4 analyses; Figure 2f) A small subset of float rocks and a large clast within a conglomerate have relatively dust-free surfaces, where we observe interlocking light and dark patches whose color does not relate to grain boundaries but instead creates (in some examples) a porphyritic texture suggestive of igneous diorites (e.g., Clinton, sol 512; Ruker, sol 387; and Reedy, sol 526). These rocks are categorized as possibly igneous because we see some textures that appear to be igneous, but we cannot exclude the possibility that these rocks are sedimentary and composed of cemented igneous phenocrysts. The name of this category is shortened to "igneous" in figure legends.

Diagenetic (36 analyses; Figure 2g) A variety of features indicating diagenetic overprinting have been identified during the traverse, including nodular concretions [*Stack et al*., 2014], raised ridges [*Léveillé et al*., 2014; *Siebach et al*., 2014], light-toned veins [*Nachon et al*., 2014], and dendritic concretions [*Grotzinger et al*., 2015; *Kah et al*., 2015; *VanBommel et al*., 2016]. Analyses collected on features that are clearly related to diagenetic fluids and preferential or replacement cementation (e.g., calcium-sulfate fracture fills [*Nachon et al*.,

2014], Mg-enriched raised ridges [*Léveillé et al*., 2014], Mn-enriched fracture fills [*Lanza et al*., 2016], and magnesium-sulfate dendritic features [*VanBommel et al*., 2016]) are categorized as diagenetic targets. Diagenetic targets clearly reflect open-system alteration, and thus, we have not used these targets to constrain source rock chemistry.

Murray mudstone (27 analyses; Figure 2h) On sol 750, *Curiosity* crossed the boundary between Bradbury group alluvial fan and delta deposits derived from the northern rim of Gale and the lacustrine mudstones of the Murray formation, the stratigraphically lowest unit of the Mount Sharp group [*Grotzinger et al*., 2015]. As a lake deposit, the mudstone may be derived from multiple sources, given that slopes transporting sediment dip from all directions toward the northern crater moat where the Murray mudstone accumulated. We include targets in the Murray formation exposed at Pahrump Hills (up to sol 860) for comparison to the Bradbury group rocks that compose the other seven categories. The Murray formation at Pahrump Hills is interpreted to be a mudstone because of its fine grain size, which is below the MAHLI limit of resolution. It is interpreted as a lake deposit due to its fine grain size, its laterally continuous millimeter-scale lamination, and its paleogeographic position downslope of delta deposits [*Grotzinger et al*., 2015]. Locally, the laminated mudstones are overprinted by diagenetic concretions and secondary crystals interpreted as evaporite mineral molds [*Grotzinger et al*., 2015; *Kah et al*., 2015; *VanBommel et al*., 2016]. Three targets within the Murray formation show coarser grain sizes, and their sedimentology is not currently well understood; these three targets are not considered further here but are included in Table S1 in the supporting information.

4.2. APXS Compositional Trends With Texture

In order to test whether target compositions vary systematically with grain size, the textural categories defined in the last section were arranged, to the extent possible, in order of increasing grain size (as noted above, analyses of "diagenetic" features were excluded from this analysis). The Murray mudstone (Mount Sharp group) and Sheepbed mudstone (Bradbury group) make up the finest-grained end-members; then the categories for which grain size can be bracketed or measured follow in order of increasing grain size: fine sandstone, sandstone, and conglomerate. The uncertain and possible igneous categories were included as coarse-grained end-members because, texturally, the uncertain category frequently looks most similar to the conglomerate category despite the lack of distinguishable grains, and the possible igneous category includes targets that are large clasts within conglomerates, which by definition are the coarsest grains. This ordering also parallels and enhances the compositional trends, as shown in Figure 3, although the trends are visible even when the uncertain and possible igneous categories are excluded.

Figure 3 shows that the elemental abundances measured by APXS (expressed as oxides, including volatiles) vary systematically with grain size, or textural category, of the Bradbury group rocks. SiO_2 (Figure 3a), Al_2O_3 (Figure 3c), and Na_2O (Figure 3e) are most enriched in the coarser-grained textural categories, whereas FeO_T (Figure 3b); MgO (Figure 3d); TiO_2 (Figure 3f); and Cr_2O_3, MnO, Ni, Zn, and Br (not shown in Figure 3) are enriched in the finer-grained textural categories (CaO, K_2O, P_2O_5, SO_3, and Cl, also not shown in Figure 3, are uncorrelated with grain size). Note that the Murray mudstone is plotted for comparison, but it is not a member of the Bradbury group and does not follow the same trends.

The Bradbury group compositional trends are most clearly defined by the variation between the fine sandstone, sandstone, conglomerate, and uncertain/possible igneous categories. Although it is the finest grain-size fraction, the Sheepbed mudstone (red in Figure 3) is not always consistent with the compositional trends established by the other textural categories. This is not necessarily unexpected because the Sheepbed mudstone—a lake sediment—is more likely to accumulate detrital inputs from multiple sources (as discussed above in the context of the Murray formation), as opposed to the more restricted sources for fluvial sediments. Similarly, the uncertain category has a wider range of compositions than the other categories (Figure 3), likely related to the incorporation of float rocks that may not all be part of the Bradbury group depositional system.

To first order, for the Bradbury group, these results indicate that the distinguishing chemical components of feldspars (Al_2O_3, SiO_2, and Na_2O) are concentrated in the coarsest-grained sedimentary rocks (the absence of an enrichment in CaO is discussed below), and the distinguishing chemical components of mafic minerals (FeO_T, MgO, and TiO_2) are concentrated in the finest-grained sedimentary rocks (although not shown in Figure 3, Cr_2O_3, MnO, and Ni follow the trends of FeO_T and MgO). These trends describe much of the

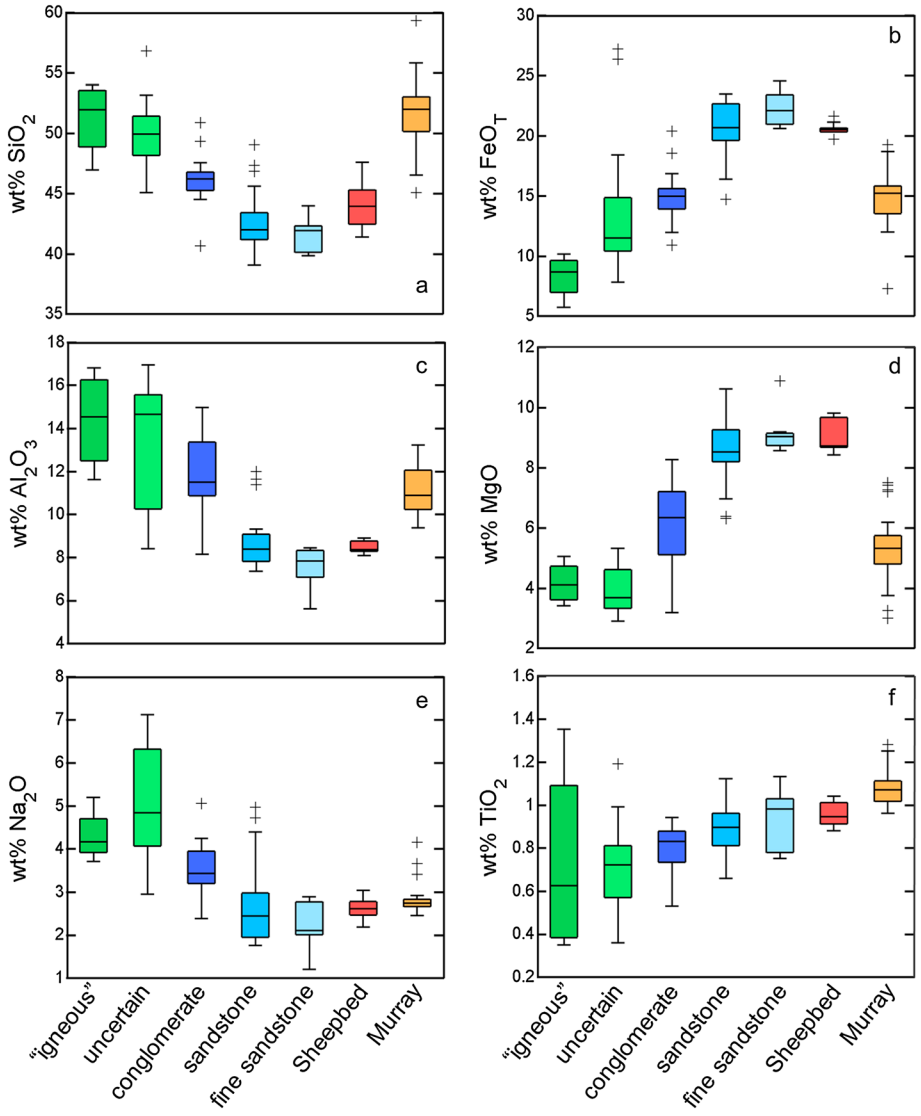

Figure 3. (a–f) Box plots showing the major-elemental compositions of each of the textural classes of Bradbury group targets ordered from coarsest grained on the left ("igneous" = possible igneous, in green) to finest grained on the right (Sheepbed mudstone, in red), plotted with the fine-grained Murray mudstone targets in orange on the far right. For each textural group, the dark central line represents the median data point; the colored box encompasses 25th and 75th percentiles; whiskers typically extend to minimum and maximum data points, but the maximum whisker length is 1.5 times the length of colored box; and plus signs demarcate the outlier points. Trends show higher concentrations of SiO_2, Al_2O_3, and Na_2O in coarser-grained textures and higher concentrations of FeO_T, MgO, and TiO_2 in finer-grained textures.

compositional variability in the Bradbury group rocks, as shown in normalized molar ternary diagrams Al_2O_3-$CaO + Na_2O$-K_2O (A-CN-K) in Figure 4a and A-CNK-FeO_T + MgO (FM) in Figure 4b. Most of the compositional variability between targets is along the feldspar-FM join in the mafic ternary plot (Figure 4b), consistent with anticorrelated proportions of mafic minerals and feldspars. This compositional variability also correlates with the target textures. Furthermore, there is no evidence for significant cation-exchange (i.e., open-system) weathering, which would drive the trends in the direction of the red arrows in Figure 4.

Figures 3 and 4 clearly indicate that composition is related to grain size in the Bradbury group. Assuming negligible open-system chemical weathering (consistent with the trends in Figure 4), this result is best explained by mechanical weathering and transport processes segregating mineral grains or lithic fragments. The next several sections consider the material being sorted and the broad compositional characteristics of the source rocks (assumed to be igneous) that are being mechanically weathered. First, we consider why K_2O does not trend with texture/grain size, and then:

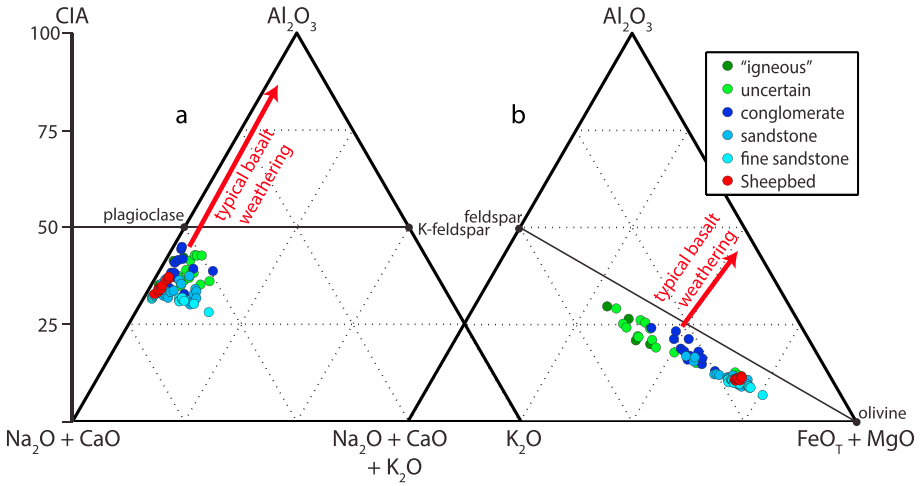

Figure 4. Molar (a) Al_2O_3-($CaO + Na_2O$)-K_2O and (b) Al_2O_3-($CaO + Na_2O + K_2O$)-($FeO_T + MgO$) ternary diagrams showing the compositions of Bradbury group rocks. Analyses of diagenetic and Murray mudstone targets have been excluded. Typical terrestrial basalt weathering trends demarcated with red arrows. Chemical Index of Alteration (CIA) scale, on left, describes the molar ratio Al_2O_3/($CaO + Na_2O + K_2O$) and is a measure of feldspar weathering.

1. Is the compositional data consistent with sorting of plagioclase grains from a relatively homogeneous protolith composition equal to average Mars crust?
2. Do the compositional trends overlap broadly with magmatic differentiation trends of terrestrial lavas, Martian shergottites, and clasts from Northwest Africa (NWA) 7533 (suggesting the sorting of lithic clasts from distinctive protoliths)?
3. What does a model that estimates igneous mineral proportions from the APXS compositional data set indicate about the broad compositional nature of the igneous rocks that provided sediments to Gale crater?

4.3. Potassium Versus Stratigraphic Elevation

Potassium is a highly incompatible element in mafic igneous systems and therefore makes a good tracer for distinctive igneous sources [*Gast*, 1968; *Engel et al.*, 1974], especially for rocks that have experienced minimal degrees of weathering [e.g., *Nesbitt and Young*, 1984]. Abundances of K_2O are particularly interesting in the Bradbury group because they do not trend with grain size/texture like the other felsic mineral components (Al_2O_3, SiO_2, and Na_2O) but instead vary independently and appear to be highly concentrated (up to 4 wt %) in a few stratigraphic intervals (average Mars crust is estimated to contain 0.45 wt % K_2O [*Taylor and McLennan*, 2009]). Figure 5 shows the variations in K_2O/Na_2O (on a weight basis) as a function of elevation, which is used here as a simple proxy for stratigraphic layering since the sedimentary layers are extremely flat lying, with measured dips of only $\pm 3°$ [*Grotzinger et al.*, 2015]. The K_2O/Na_2O values generally lie between ~0.15 and 0.5 with minor perturbations to higher values; for reference, K_2O/Na_2O values for average Mars crust, average Martian soil, Gale crater soil, and shergottites are 0.15, 0.16, 0.20, and 0.09, respectively [*Taylor and McLennan*, 2009; *Meyer*, 2015; *Treiman and Filiberto*, 2015; *O'Connell-Cooper et al.*, 2016] (shergottite ratio based on average K_2O and Na_2O values). However, in the Bradbury group rocks, K_2O/Na_2O increases dramatically, up to a value of 2.5, in targets measured at the Kimberley outcrop at an elevation of −4480 m [*Thompson et al.*, 2014; *Le Deit et al.*, 2016; *Thompson et al.*, 2016].

The high potassium contents (>2 wt % K_2O) found in targets analyzed in the vicinity of the Kimberley outcrop span most of the textural categories defined above: fine sandstone, sandstone, conglomerate, and uncertain, and there appears to be no clear correlation between these textural categories and potassium abundances for these targets (if such a trend exists, it is currently being obscured by limited sampling over the narrow range of relevant elevations). The Windjana target, a fine sandstone drilled at the Kimberley outcrop, contains 21% potassium feldspar by weight in the form of sanidine based on CheMin X-ray diffraction data [*Treiman et al.*, 2016]. The presence of abundant sanidine in the drilled

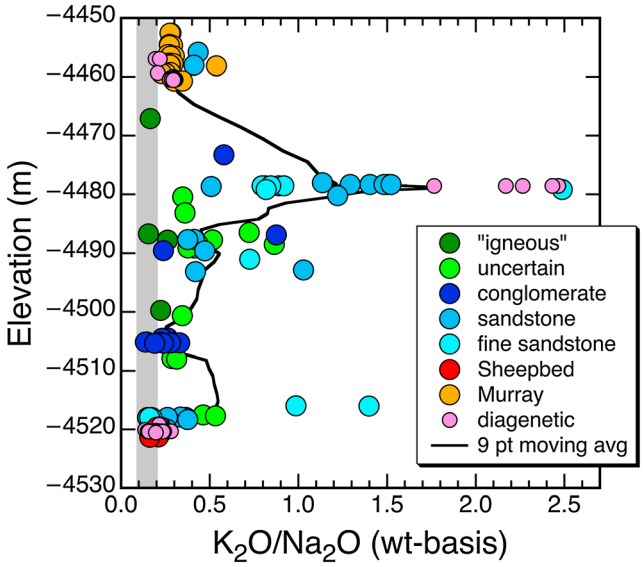

Figure 5. K_2O/Na_2O (weight basis) versus elevation (in meters) for the APXS rock analyses, including diagenetic samples, listed in Table S1. Black line is a 9 point moving average with elevation. Vertical gray band denotes the range in K_2O/Na_2O values for average Martian soil [*Taylor and McLennan*, 2009], average Gale crater soil [*O'Connell-Cooper et al.*, 2016] and dust [*Berger et al.*, 2016], and the average for shergottites (based on average Na_2O and K_2O contents from *Treiman and Filiberto* [2015] and the Martian Meteorite Compendium [*Meyer*, 2015]).

Windjana targets at Kimberley (inferred to be of igneous origin [*Treiman et al.*, 2016]) strongly suggests that more evolved rocks contributed sediments to the Windjana site since terrestrial examples of sanidine of the composition inferred from the CheMin data (~Or_{95} [*Treiman et al.*, 2016]) have only been found in rare leucite lamproites (also called orendites [*Carmichael et al.*, 1974, p. 273]) (however, we note that more recent estimated alkali-feldspar compositions from CheMin samples in the Murray formation are much more sodic; Rampe, personal communication). The presence of significant alkali-feldspar and pigeonite in the same target requires that at least two igneous sources contributed to this sediment, including one potassium-enriched sediment source and at least one mafic source that contributed the olivines and pyroxenes [*Treiman et al.*, 2016]. The flux of sediment from this sandine-enriched igneous source may correlate with variations in K_2O throughout the Bradbury group stratigraphy, particularly in targets with K_2O/Na_2O ratios above ~0.2. Characteristics of this sanidine source are discussed further below; however, the lack of correlation between this K_2O-rich sediment flux and the major-element compositional trends in the Bradbury group indicate that this source only has a secondary effect on the geochemistry of the group as a whole.

4.4. Modeling the Compositional Trends of the Bradbury Group

4.4.1. Comparing Data With Predicted Mixing Lines

Our initial set of calculations tests the hypothesis that the compositional variability in the Bradbury group sedimentary rocks reflects the separation of coarser-grained plagioclase from the finer-grained mafic portion of an "average" Martian basalt. The starting point for these calculations is average Mars crust [*Taylor and McLennan*, 2009], although we use average Mars soil as a proxy because average Mars crust is reported on a S- and Cl-free basis, whereas the observed nondiagenetic targets have SO_3 and Cl concentrations up to 9.6 and 1.9 wt %, respectively (absolute differences between average crust and S- and Cl-free normalized average soil in major and minor oxides are ≤0.06 wt % [*Taylor and McLennan*, 2009]). Although APXS and ChemCam measurements at Gale indicate that the local Noachian crust may be more alkaline than average [*Stolper et al.*, 2013; *McLennan et al.*, 2014; *Treiman et al.*, 2016], the composition of Gale crater soil [*O'Connell-Cooper et al.*, 2016] is quite similar in its Na_2O and K_2O contents compared to average Martian soil [*Taylor and McLennan*, 2009], so average Martian soil is an acceptable compositional starting point for these calculations.

The range of modeled plagioclase end-member compositions ($An_{30–40}$) were selected to encompass a reasonable range based on orbital, CheMin, and ChemCam observations. These include the normative plagioclase composition for average Martian crust, An_{34}; CheMin analyses of a Sheepbed mudstone and the K-rich sandstone Windjana, ~$An_{35–45}$ [*Vaniman et al.*, 2014; *Treiman et al.*, 2016] (Morrison, personal communication); and trends in ChemCam analyses of Bradbury group rocks in SiO_2-Al_2O_3 space, which are consistent with plagioclase compositions of $An_{30–40}$ [*Mangold et al.*, 2016]. Figure 6 shows, in oxide-MgO space, the mixing lines between An_{30} or An_{40} plagioclase and average Martian soil. The plagioclase-poor end-member compositions (black and gray squares) were calculated by removing the maximum possible amount of An_{30}

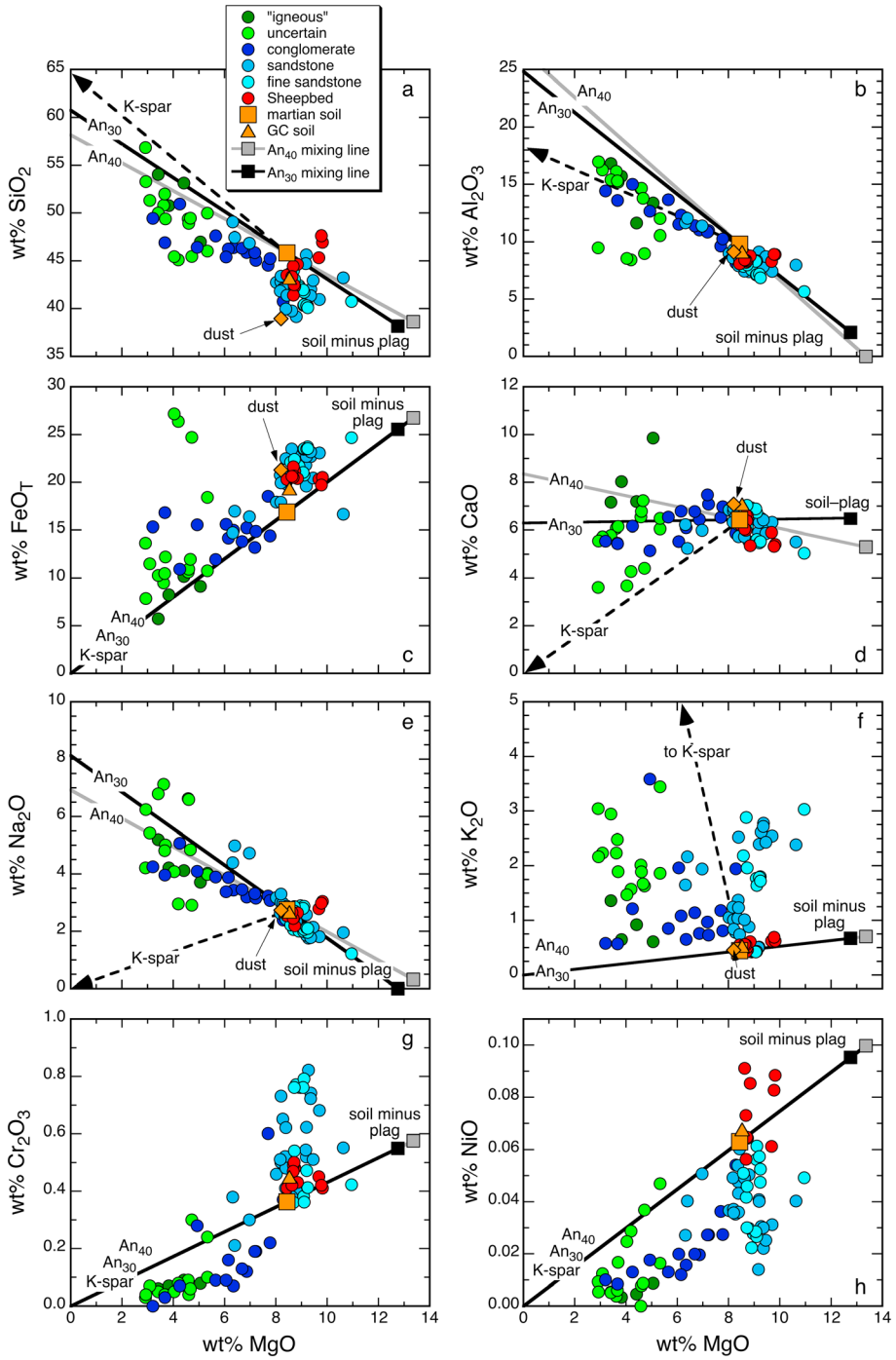

Figure 6. Nondiagenetic Bradbury group targets, average Mars soil [*Taylor and McLennan*, 2009], Gale crater soil [*O'Connell-Cooper et al.*, 2016], and dust [*Berger et al.*, 2016] in oxide-MgO space: (a) SiO_2, (b) Al_2O_3, (c) FeO_T, (d) CaO, (e) Na_2O, (f) K_2O, (g) Cr_2O_3, and (h) NiO. Solid lines show the compositional effect of adding and subtracting An_{40} and An_{30} plagioclase to and from average Mars soil; dashed line points to K-feldspar (in Figures 7c, 7f, 7g, and 7h, two or more of the lines are coincident). Gray and black squares are the compositions that represent the maximum amount of plagioclase that can be removed from average Martian soil. Cr_2O_3 and NiO contents were not determined for the Gale crater dust.

plagioclase (0.339 wt %) or An_{40} plagioclase (0.369 wt %) from average Martian soil, such that all oxides remained ≥zero; the plagioclase-rich ends of the lines are defined by the plagioclase compositions. Also plotted in Figure 6 are current best estimates of the soil composition in Gale crater [*O'Connell-Cooper et al.*, 2016] and the composition of dust that has settled on the rover's science observation tray [*Berger et al.*, 2016].

Figure 6 shows that for all oxide-MgO pairs except K_2O-MgO, the compositional trends of the sediments are broadly consistent with the addition and subtraction of $An_{30–40}$ plagioclase from average Martian soil. Furthermore, the compositions of the sandstones and conglomerates are consistent with these coarser-grained end-members being enriched in plagioclase relative to the finer-grained sandstones and the Sheepbed mudstones; this relationship also holds for the minor elements Cr and Ni. Note also that the plagioclase mixing lines are nearly horizontal in CaO-MgO space (Figure 6d), explaining the absence of a correlation between the textural categories and CaO contents of the Bradbury group rocks.

Some of the minor systematic offsets between the plagioclase mixing lines and the Gale crater targets are related to compositional differences between average Gale crater soil and average Mars soil. Although the soils are quite similar in most oxides (e.g., Figures 6b, 6e, and 6f), Gale soil is slightly depleted in silica and enriched in iron (Figures 6a and 6c) relative to average Mars soil, so the offsets in these elements would be minimized if the mixing lines were calculated using Gale crater soil. Nevertheless, both soils have similar Al_2O_3 and Na_2O contents (Figures 6b and 6e) and thus similar limits on the amounts of $An_{30–40}$ plagioclase that can be subtracted from them, so the locations of the end points of the plagioclase addition and subtraction lines in Figure 6 would not change.

There is appreciable scatter about the plagioclase addition and subtraction lines, indicating that other components beside plagioclase must have contributed to varying degrees to the compositions of these rocks [e.g., *McLennan*, 2000]. This scatter does not appear to simply reflect variations in SO_3 and Cl abundances among the different targets; deviations about the plagioclase addition and subtraction lines in SiO_2-Al_2O_3, FeO_T, and Na_2O and MgO-SiO_2, Al_2O_3, and FeO_T space are comparable irrespective of whether all the rock and soil compositions include S and Cl or are normalized on a S- and Cl-free basis. Furthermore, the fact that the composition of dust is also generally similar to that of the soils (SiO_2 and FeO_T are exceptions; Figures 6a and 6c) means that varying degrees of "contamination" of APXS analyses by dust will tend to reduce compositional spread in oxide-MgO space, minimizing trends, since mixtures of rock plus dust lie on vectors that point to dust. A few of the scattered points, however, reveal additional components that are not being incorporated into the simple plagioclase addition/subtraction model. For example, in Figure 6c, three "uncertain" targets have elevated FeO_T values suggesting enrichment in a Fe component; also, Figure 6f shows that the vast majority of the rocks have elevated K_2O contents consistent with the addition of K-feldspar as discussed in the previous section (the addition of K-feldspar also helps to explain the systematic offset in Figure 6b).

4.4.2. Deriving End-Member Characteristics From Data Regression

In an effort to further characterize the extent to which the observed bulk rock compositional variations seen in Figure 6 reflect variations in the modal abundance of feldspar, we fit robust regression lines in oxide-MgO space to all the Bradbury group nondiagenetic rock compositions and calculated the composition of the regression-line-based felsic end-member using a mass balance model. Regression lines were calculated by minimizing the sum of the absolute values of the deviations [*Press et al*., 1992, chapter 15]. Plotted as a function of MgO (Figure 7), the slopes of the regression lines are qualitatively consistent with the conclusions drawn from Figure 6: oxides enriched in feldspars relative to the mafic end-member of the trends (i.e., average soils) are inversely correlated with MgO (SiO_2, Al_2O_3, Na_2O, and K_2O; Figures 7a, 7c, 7g, and 7h); conversely, those oxides that are not essential structural constituents of feldspars (TiO_2, FeO, MnO, and MgO; Figures 7b, 7d, and 7e) are positively correlated with MgO. The near-horizontal CaO-MgO regression line (Figure 7f) would suggest that the average composition of the modally variable feldspar is andesine, consistent with the conclusions drawn from Figure 6.

The regression lines allow us to calculate the composition of a hypothetical feldspar-rich end-member (at MgO = 0 wt %) and to explore, via mass balance, what combinations of phases can reproduce this end-member composition. The composition is dominated by plagioclase and alkali-feldspar components: SiO_2, Al_2O_3, CaO, Na_2O, and K_2O comprise ~92 wt % of the bulk. Nevertheless, TiO_2 (0.52), FeO_T (1.76), P_2O_5 (0.71), SO_3 (2.34), and Cl (0.67; all in wt %) are not zero (NiO and Cr_2O_3 concentrations are negative and were set to zero). This suggests that sorting between feldspar and other detrital phases has been imperfect (to account for the nonzero concentrations of TiO_2, FeO_T, P_2O_5, SO_3, and Cl in the mass balance fit, we included ilmenite, apatite, Fe-sulfate, and halite). The best fit composition for the felsic end-member, denoted by the red diamond at MgO = 0 in Figure 7, lies within the ±bounds of the regression line (± 1 mean absolute deviation, MAD) for all oxides except P_2O_5 (0.30) and Cl (0.11) (not shown in Figure 7; values in parentheses are the

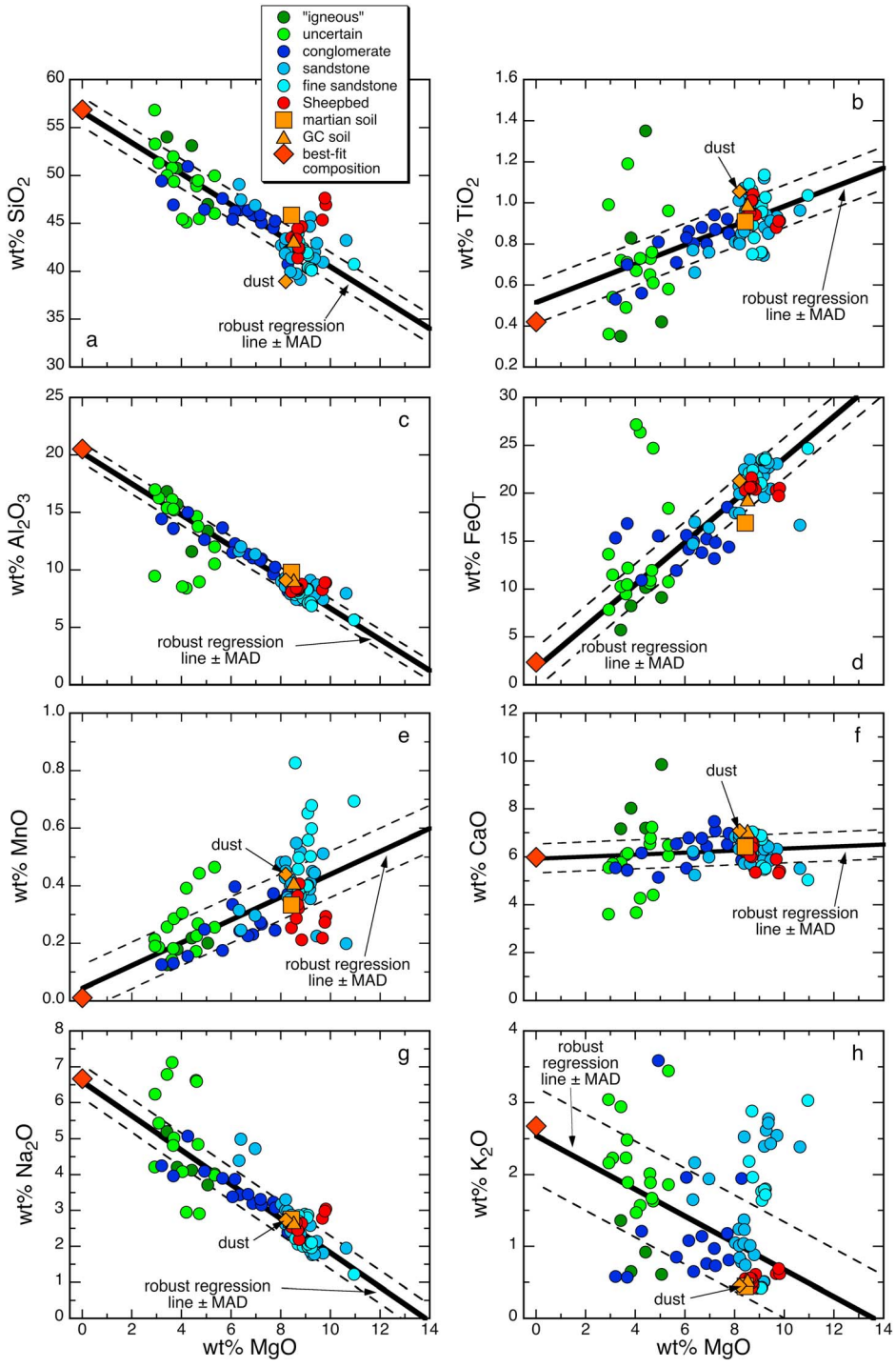

Figure 7. Nondiagenetic Bradbury group targets, average Mars soil [*Taylor and McLennan*, 2009], Gale crater soil [*O'Connell-Cooper et al.*, 2016], and dust [*Berger et al.*, 2016] in oxide-MgO space: (a) SiO_2, (b) TiO_2, (c) Al_2O_3, (d) FeO_T, (e) MnO, (f) CaO, (g) Na_2O, and (h) K_2O. Solid line is a robust fit to the Gale crater rock compositions (dashed lines are ±the mean absolute deviation); the robust lines were used to calculate an end-member mixing composition at MgO = 0. Reddish-brown diamond is the unweighted best fit (calculated using a set of mineral compositions) to that end-member composition. See text for further discussion.

differences in wt % between the calculated best fit composition and the closer of the two dashed error bounds. The best fit phase proportions indicate that plagioclase, K-feldspar, and silica comprise ~90% of this zero-MgO end-member (in weight fractions: ~0.70 plagioclase, 0.17 K-feldspar, and 0.03 silica).

The calculated An content of the plagioclase is ~An_{30}, a value broadly consistent with CheMin and ChemCam data discussed above. Assuming a more sodic K-feldspar composition, e.g., Or_{60} versus Or_{95} (as observed by CheMin in the Murray formation; Rampe, personal communication) changes the calculated plagioclase composition to ~An_{35}, and feldspars + silica still constitute ~90% of the best fit solution.

The fact that plagioclase is the most abundant phase in this calculated end-member composition is consistent with our initial analysis shown in Figure 6. It is also significant that silica comprises only 3% of the phases—a point we will return to in section 5.3. Finally, although MgO and K_2O are inversely correlated (Figure 7h), the calculated mass fraction of alkali-feldspar represents an average value. As shown in Figure 7h, K_2O concentrations in the uncertain and sandstone rock categories form trends at high angles to the regression line and the Sheepbed mudstones and some of the sandstones and fine sandstones appear to contain little to none of this phase, while others (e.g., the conglomerate with ~3.6 wt % K_2O) must contain nearly 32 wt % alkali-feldspar if it is assumed to be pure orthoclase/sanidine. The same simple calculation applied to the Windjana dust removal tool (DRT) target (Table S1 and supporting information) yields 24 wt % K-feldspar, a value that overlaps with the CheMin determination of 21 ± 3 wt %. As discussed in section 4.3, most of these K_2O-rich rocks are from the vicinity of the Kimberley outcrop.

4.5. Comparison With Igneous Evolution Trends

Previous work has suggested that the compositional diversity of the Bradbury group rocks requires extensive igneous diversity in the source region [*Sautter et al*., 2015; *Sautter et al*., 2016; *Treiman et al*., 2016]. The principle compositional variation can be described in terms of sediments with either more felsic or more mafic components, which, although interpreted here as sorting of minerals derived from a relatively homogeneous provenance, could also result from poor sorting of lithic fragments originating from lavas of variable compositions, perhaps in a sequence of basaltic to more felsic compositions (as observed, for example, on many ocean islands). Indeed, in terrestrial volcanic terrains, lithic fragments are often the dominant sedimentary component as opposed to mineral grains of quartz or feldspar [e.g., *Marsaglia*, 1993; *Cox and Lowe*, 1995; *Smith and Lotosky*, 1995]. Changes, as a function of time, in the surface-area weighted average of the composition of the igneous rocks in the source region of the sediments may produce compositional variations in a stratigraphic sequence of sediments. A prerequisite to attributing the Bradbury group compositional trends to the mixing of lithic clasts from broadly related igneous rock suites would be to show examples of magmatic suites that parallel the Bradbury group compositional trends as they transition from mafic to felsic lavas. Here we explore whether there are known terrestrial or Martian suites of igneous rocks that substantially overlap the compositional trends of the sedimentary rocks of the Bradbury group.

Primitive terrestrial basalts with more than 14 wt % FeO_T are rare in the geologic record [*Milidragovic and Francis*, 2016], and thus, the vast majority of terrestrial tholeiitic, calc-alkaline, and alkaline suites of rocks have FeO_T contents that are too low to match those of Martian basalts in general and the more MgO-rich Gale crater rocks in particular. An exception, as noted by *Filiberto* [2008], are Archean ferropicrites and associated rocks, and Figure 8 compares the examples of these Fe-rich terrestrial rocks from the Superior, Slav, and West Churchill cratons in Canada [*Milidragovic and Francis*, 2016] to the Bradbury group sedimentary rocks. Also shown in Figure 8 are the bulk compositions of shergottites [*Meyer*, 2015, and references therein; *Treiman and Filiberto*, 2015]; clasts from NWA 7533 [*Humayun et al*., 2013]; and, although their FeO_T contents are too low, alkaline lavas from ocean islands so as to compare their Al_2O_3-MgO trends with that of the Martian targets.

The Neoarchean ferropicrites and associated rocks from Canadian cratons [*Milidragovic and Francis*, 2016] broadly overlap, albeit with substantial scatter, the Bradbury group rocks in Figure 8a (in the following discussion, the term "ferropicrite" will be applied to all of the Neoarchean rocks plotted in Figure 8 irrespective of their MgO content). However, FeO_T and MgO contents are inversely correlated in these rocks in striking contrast to the positive correlation between these two oxides in the Bradbury group targets (Figure 8b). Even considering "ferropicrites" with MgO contents between 3 and 11 wt % (the range exhibited by the Bradbury rocks), FeO_T and MgO still show a statistically significant inverse correlation (Spearman rank-order correlation coefficient, $r_S = -0.27$). In contrast to the broad scatter of the ferropicrite

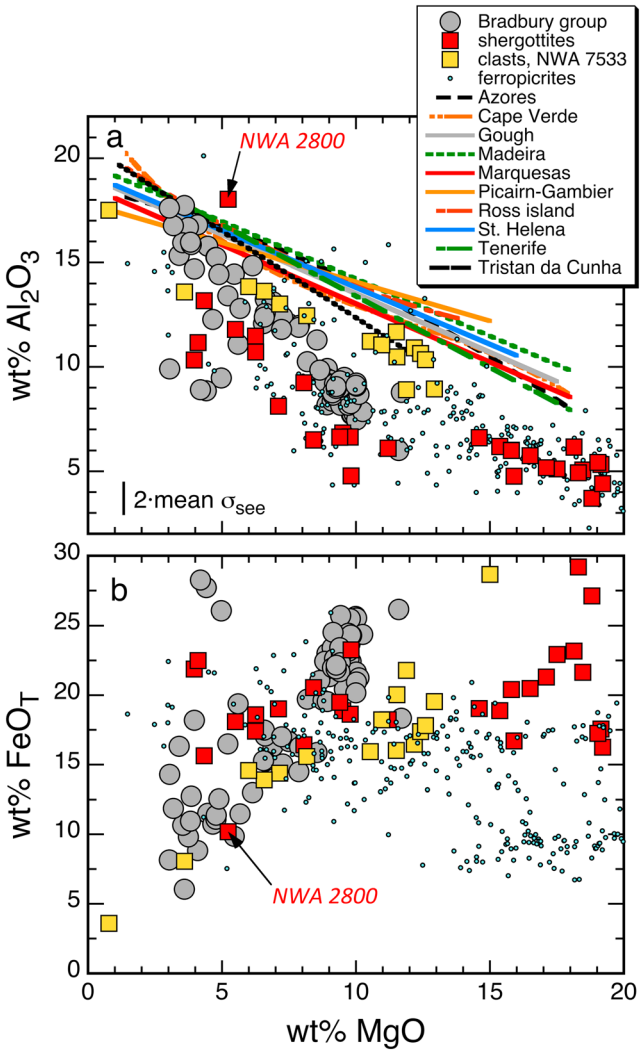

Figure 8. Martian and terrestrial igneous rock compositions compared to those of the Bradbury group in (a) Al_2O_3-MgO and (b) FeO_T-MgO. Shergottite data from *Treiman and Filiberto* [2015] and the *Martian Meteorite Compendium* [*Meyer*, 2015], NWA 7533 clast compositions from *Humayun et al*. [2013], ferropicrite compositions from *Milidragovic and Francis* [2016], and compositions of ocean island lavas (Azores to Tristan da Cunha from Georoc: http://georoc.mpch-mainz.gwdg.de/georoc/) were fit to linear or second- or third-order polynomials in an effort to minimize "clutter" in Figure 8a. The short vertical bar in Figure 8a is twice the mean standard error of the estimate based on all of the ocean island fits. NWA 2800 is a coarse-grained and unusually plagioclase-rich shergottite (thus, its high Al_2O_3 content is relative to other shergottites).

rocks in Figure 8a, compositions of generally alkaline lavas (basanites/basalts to phonolites/trachytes) from ocean islands define narrow linear to near-linear trends in Al_2O_3-MgO space. These trends are shallower than the trend of the Bradbury group rocks and intersect it at ~3–4 wt % MgO (note the size of the mean standard error of estimate based on all of the ocean island fits; Figure 8a). The monotonic increase in Al_2O_3 with fractionation reflects the suppression of plagioclase crystallization due to the relatively high water contents of these ocean island magmas (under anhydrous condition and at relatively low pressures, plagioclase would join the crystallizing assemblage at ~5 wt % MgO and cause Al_2O_3 contents in the evolving liquids to decrease with increasing fractionation [e.g., *Stolper et al*., 2013]). Petrologic and experimental data on alkaline rock series like those plotted in Figure 8a generally indicate that magmatic water contents are in the range of ~3–6 wt % and that fractional crystallization of the more primitive magmas occurs at the base of the crust or in midcrustal magma chambers while fractionation of the more evolved magmas occurs at pressures of ~0.5–2 kbar [e.g., *Ablay et al*., 1995; *Andújar et al*., 2010; *Andújar and Scaillet*, 2012, and references therein] (on Mars, pressures of 0.5–2 kbar would correspond to depths of 5–17 km). The magmas of Mt. Erebus are an exception, evolving under relatively dry conditions—experimental phase equilibria suggest that these melts contain $<$1–2 wt % H_2O [*Moussallam et al*., 2013; *Iacovino et al*., 2016]. The fact that a relatively wide range of crystallization pressures and magmatic water contents has nevertheless produced a tight clustering of the Al_2O_3-MgO trends for alkaline rocks in Figure 8a suggests that there are unlikely to be P-T-P_{H2O} conditions that will produce a steeper Al_2O_3-MgO trend for such magmas— i.e., one that more closely parallels or overlaps the trend of the Bradbury group rocks.

Although lavas from the terrestrial ocean islands define suites that are comagmatic, this is not the case for the shergottites [e.g., *Shearer et al*., 2008; *McSween and McLennan*, 2014] and, in all likelihood, the clasts in NWA 7533 and 7034 [*Humayun et al*., 2013; *Santos et al*., 2015]. Nevertheless, both of these latter two groups of rocks/clasts define broadly coherent major-element compositional trends, and for the purposes of the

discussion here, it is the existence of these compositional trends, and the fact that such trends could potentially have existed in the watershed that supplied sediments to Gale crater, that is important. It is also significant that zircons from NWA 7533 yield crystallization ages of ~4.4 Ga [*Humayun et al*., 2013; *Yin et al*., 2014], indicating that the very early crust of Mars contained both basaltic and more felsic compositions. Although the "basaltic" shergottites (<~12 wt % MgO) and the NWA 7533 clast compositions either parallel or partially overlap with the Bradbury group targets in Al_2O_3-MgO and FeO_T-MgO space, the trends are either sufficiently offset or rotated so that lithic fragments from source rocks similar in composition to either of these two rock groups would not reproduce the compositional trends of the Gale crater targets. (The dramatic increase in Al_2O_3 with decreasing MgO in the basaltic shergottites reflects the fact that plagioclase is not a near-liquidus phase in the more primitive basaltic shergottites due to their very low bulk Al content; i.e., water is not necessarily required to suppress plagioclase crystallization. NWA 2800, a very course grained target [*Meyer*, 2015], is extremely rich in modal "plagioclase." Given the apparent absence of terrestrial or Martian igneous rock compositional trends that match those of the Bradbury group rocks, we tentatively conclude that the observed compositional trends of these rocks do not reflect mixing of lithic fragments.

4.6. Modeling APXS Mineralogy

Typically, terrestrial rocks are characterized by a combination of mineralogy and bulk chemistry, but, due to sampling limitations with the rover, mineralogical phase assemblages and estimates of mineral chemistry are only available for 3 of the 73 distinct rocks in Aeolis Palus that have been analyzed by APXS. For igneous rocks where only a bulk chemical analysis is available, estimates of the mineral phase assemblage and proportions of phases can be made using a number of different methods, the most common of which is the CIPW norm [e.g., *Kelsey*, 1965] (see *Rittmann* [1973] and *Ragland* [1989] for a discussion of other normative calculation schemes). The CIPW norm transforms a chemical composition into a set of anhydrous end-member minerals following a set of rules that approximates the crystallization sequence of an anhydrous magma under plutonic conditions. However, in the case of sediments, like the Aeolis Palus rocks, "equilibrium crystallization" constraints do not apply since these rocks are composed of a collection of mineral grains from an unknown number of igneous source rocks, and thus, the compositions of the sediments are not constrained by phase equilibria. Efforts to calculate the mode of a sedimentary rock given only its bulk composition involve either normative schemes using end-member minerals that include clays or least squares methods that attempt to reproduce the bulk composition using the compositions of minerals commonly found in clastic sedimentary rocks [e.g., *Garrels and Mackenzie*, 1971; *Cohen and Ward*, 1991; *Laube et al*., 1996]. The hybrid approach of *McSween et al*. [2010] to estimate the modal mineralogy of Martian soils used both MiniTES data to constrain the proportions of the assumed alteration phases, including silica and idealized nontronite and montmorillonite, and a CIPW norm (with Fe^{3+}/Fe_T from Mössbauer data) to account for the igneous minerals in the remaining portion of the bulk composition. Our approach uses a least squares method, but we assume that the clays and amorphous components present in the targets analyzed by CheMin (and likely to be universally present in the Aeolis Palus rocks) are not the products of extensive open-system weathering of the sediments but are instead related to postdepositional cation-conservative alteration (an assumption supported by Figure 4) [see also *McLennan et al*., 2014]. If this last assumption is correct, then the bulk compositions can potentially be modeled using mixtures of primary igneous minerals without calling upon any alteration phases such as clays. The advantage of our mass balance approach over the CIPW normative scheme is that (1) we can select a specific set of igneous phases based on CheMin results, (2) the mineral compositions in our mass balance routine are "realistic" in that they have major and minor element concentrations consistent with phase compositions in Martian meteorites, and (3) sedimentary rock analyses that fail mass balance at the 95% confidence level can be "flagged" as indicating that those rocks have potentially experienced some form of open-system alteration.

4.6.1. Methods

In order to estimate the mineralogy of the Bradbury rock compositions and test the assumption of minimal open-system chemical weathering for those targets that do not show visible evidence of diagenetic overprinting, we use a Monte Carlo-based mass balance model to test whether the rock compositions as determined by APXS are consistent with a mixture of primary igneous minerals whose compositions are, in turn, constrained by the compositions of phases in Martian meteorites [e.g., *Papike et al*., 2009; *Gross et al*., 2011; *Santos et al*., 2015; *Wittmann et al*., 2015] and by the CheMin data for three

Gale crater-drilled targets [*Vaniman et al*., 2014; *Morrison et al*., 2015; *Treiman et al*., 2016]. The minerals included in the calculations are olivine, high- and low-Ca pyroxene, plagioclase, K-feldspar, apatite, ilmenite, chromite, iron oxide (FeO_T as a proxy for magnetite), and silica (we recognize that iron oxide and silica may be both igneous and alteration phases). The mass balance calculation attempts to find the best set of phase proportions in a least squares sense that minimizes deviations between the calculated bulk composition and the measured bulk composition for the following oxides: SiO_2, TiO_2, Al_2O_3, Cr_2O_3, FeO_T, MnO, MgO, CaO, Na_2O, K_2O, P_2O_5, and NiO (all compositions are normalized on a S- and Cl-free basis; this is justified in Appendix A1 and Appendix A2). While mass balance calculations are widely used in petrology [e.g., *Bryan et al*., 1969; *Reid et al*., 1973; *Walter et al*., 1995], their application to the mixing problem discussed here is complicated by the fact that we have very limited information on the compositions of the major phases [*Vaniman et al*., 2014; *Morrison et al*., 2015; *Treiman et al*., 2016]. However, using the compositions of mineral phases in Martian meteorites and mineral stoichiometric constraints [see *Baker and Beckett*, 1999], we can construct, using random numbers, a population of stoichiometric olivines, pyroxenes, plagioclases, etc., whose compositions are consistent with those of Martian meteorites, and, pulling phase compositions from these populations, run a very large number of mass balance calculations (5,000,000; i.e., 25 runs of 200,000 calculations per run) for each target. Details of the mass balance calculations are given in Appendix A2, including the results of calculations using a set of synthetic compositions of known mineral proportions (based on the textural categories described in this work) to test the accuracy of the model.

Although a large majority of the APXS sedimentary rock compositions can be modeled using only the compositions of igneous minerals that are consistent with those in Gale crater rocks (as estimated by CheMin) and found in Martian meteorites, this does not mean that these sedimentary rocks are necessarily composed of just these phases. Indeed, based on the results of the small number of CheMin X-ray diffraction (XRD) analyses, there may well be clay minerals and one or more difficult-to-characterize amorphous phases in all of the Gale crater sedimentary rocks [*Vaniman et al*., 2014; *Treiman et al*., 2016]. It does suggest, however, that the compositions of the materials that accumulated to produce these sedimentary rocks can be described as mixtures of igneous minerals and that a substantial loss of cations following deposition has probably not occurred. Calculations using bulk compositions of progressively more severely weathered basaltic rocks [*Chesworth et al*., 1981; *Nesbitt and Wilson*, 1992; *Sheldon*, 2003] show that mass balance fits generally fail at the 95% confidence level once the CIA value exceeds ~50–55. Furthermore, if the mass balance calculations indicate the presence of pigeonite as a significant modal phase in many of the rocks, that has important implications for interpreting source rock compositions—pigeonite does not crystallize during the low-pressure fractionation of nepheline-normative basalts [e.g., *Wilkinson*, 1967; *Miyashiro*, 1978; *Sack et al*., 1987].

4.6.2. Results

The results of all 138 mass balance calculations are reported in Table S3; nine analyses of four rocks (also listed in Table S3) were not mass balanced due to either their high SO_3 or MnO contents (~12.5–28 or 3.4–4.9 wt %, respectively). For all of the targets, either the best fit calculations from a set of 25 runs were all statistically significant at the 95% confidence level or they were all not successful. Phase proportions for the 117 analyses that yielded successful mass balance fits summed to between 0.988 and 1.018 (they were not forced to sum to 1), suggesting that our selected assemblage of anhydrous mineral phases is sufficient to capture the compositional variation in these 117 analyses. Out of 83 nondiagenetic rock analyses, 74, or about 90% of the nondiagenetic Bradbury group analyses, were successfully modeled as sums of primary igneous minerals with Q values $\geq$0.05. This is consistent with the assumption of minimal weathering and generally cation-conservative alteration (Figure 4) [*McLennan et al*., 2014] and further confirms those results by showing that all of the elements that were included in the model (with the exception of Ni, discussed below) can be accommodated in primary igneous minerals in the vast majority of the Bradbury group rocks. This does not preclude the formation of secondary minerals or the presence of amorphous phases—indeed, these phases are present in each of the targets analyzed by CheMin—but simply indicates that the compositions are consistent with cation-conservative authigenesis rather than extensive open-system weathering. Important caveats to these statements are we have not modeled S and Cl, some fraction of the calculated "FeO" component may be diagenetic, and Ni contents in many of the rocks are elevated over what would be expected based on the calculated mass fractions of olivine and pyroxenes, suggesting a nonigneous Ni-rich component in many of the rocks (e.g., meteoritic material [*Yen et al*., 2006]). Since the primary focus here concerns variations

in plagioclase abundance as a function of grain size, we defer a discussion of issues like those of Ni to the paper that will present the details of the mass balance model.

In eight of the nine Bradbury group analyses that could not be modeled at the 95% confidence level (Jake_Matijevic, three analyses; Stirling; JumJum; Oscar; Morehouse; and Secure), the misfit between measured and calculated Na_2O contents accounts for between 50 and 78% of the total χ^2 value—in all cases, the measured bulk sodium concentration is high relative to the calculated value. The most Na_2O-rich phase in the mass balance calculation is plagioclase, which is allowed to vary from An_{20} to An_{70}. The three Jake_Matijevic compositions, Stirling, JumJum, and Morehouse, still "fail" the mass balance even if the lower limit on the plagioclase compositional bound is set to An_0 (Oscar and Secure "pass," although the best fit plagioclase is essentially pure albite). This suggests that another sodium-rich but Al-poor phase is present in these targets—this could be "altered" Na-rich glass, especially if its composition is peralkaline. Note that all of these compositions are nepheline-normative (3.3–18.4 wt %; CIPW norms calculated with all Fe as FeO_T for consistency with the mass balance calculations); nevertheless, among the rock compositions that mass balance, normative nepheline ranges from 0 to ~11 wt %, and thus, the presence of normative nepheline does not preclude a successful fit. Finally, the enrichment does not reflect a contribution from dust since the composition of Martian dust [*Berger et al*., 2016] has a lower Na_2O content than that in all eight of these rock analyses. The ninth composition, Windjana DRT, fails the mass balance calculation due to its high MnO content (~0.7 wt %); the mismatch between the measured and calculated MnO values accounts for >55% of the total χ^2 value. The proximity of Windjana to the Stephen target that contains between 3.4 and 4.9 wt % MnO strongly suggests that there has been an influx of Mn into the Windjana unit that was analyzed by APXS and targeted by CheMin.

Only 16 of the 27 analyses of the Murray mudstones were fit at the 95% confidence level, suggesting that a larger fraction of Murray targets have been affected by open-system chemical weathering or some form of chemical alteration compared to the Bradbury group rocks. All of the successful mass balance calculations of Murray targets required a free silica phase (with calculated abundances varying from ~3 to 21%; Table S3). This contrasts with the 73 Bradbury group rocks where only 2 targets required free silica (~7–8 wt %) for a successful fit. In 9 of the 11 Murray analyses that yielded poor fits, mismatches between measured and calculated Al_2O_3 and Na_2O contents account for between ~69 and 81% of the total χ^2 values—measured Al_2O_3 concentrations were high and Na_2O contents were low. Since Al is considered to be relatively immobile during terrestrial weathering [e.g., *Nesbitt*, 2003], one interpretation of these results is that Na has been lost from these targets. For the remaining two targets that failed mass balance, the high measured P_2O_5 contents compared to calculated phosphorus concentrations account for 83 and 90% of the total χ^2 values (note that P_2O_5 contents in the other nine analyses are also high relative to calculated values), suggesting an influx of P in many of the Murray mudstones or the presence of a P-rich phase that does not have a high Ca content. These mass balance results are consistent with previously published reports showing that the Murray mudstone sediments have been more affected by some form of chemical weathering than the mudstones of the Bradbury group [*McLennan et al*., 2015].

The diagenetic targets were categorized as such because they contain textural features showing preferential cementation and we did not attempt to mass balance nine analyses because they exhibited either very high SO_3 contents (~12.5 to 28 wt %) or contained MnO contents between 3.4 and 4.9 wt % (all of the analyses of Stephen)—far outside the range of MnO values that can be accounted for by any collection of igneous mineral compositions that have been analyzed in Martian meteorites. The remaining 28 analyses were successfully mass balanced using the compositions of igneous minerals. Although this may seem surprising at first glance, given the visual evidence of sulfate addition, the SO_3 contents of these 28 analyses are generally comparable to those of the Murray mudstones and the Bradbury group rocks. Renormalizing on a S-free basis the compositions of rocks that have experienced the addition of $CaSO_4$ cement, for example, simply leads to an increase in CaO that can be accounted for by a decrease in the pigeonite to augite ratio. The extent to which this adjustment in the modal proportions of the low- and high-Ca pyroxenes can accommodate the "excess" CaO is, in part, a function of the bulk SiO_2/CaO ratio and bulk Al_2O_3 (the Al content controls the modal abundance of plagioclase, the other major reservoir of Ca among anhydrous igneous phases). Preliminary calculations using a set of synthetic compositions (see Appendix A2) suggest that the pigeonite/augite ratio is quite sensitive to added "$CaSO_4$"—the addition of 8% calcium sulfate to the

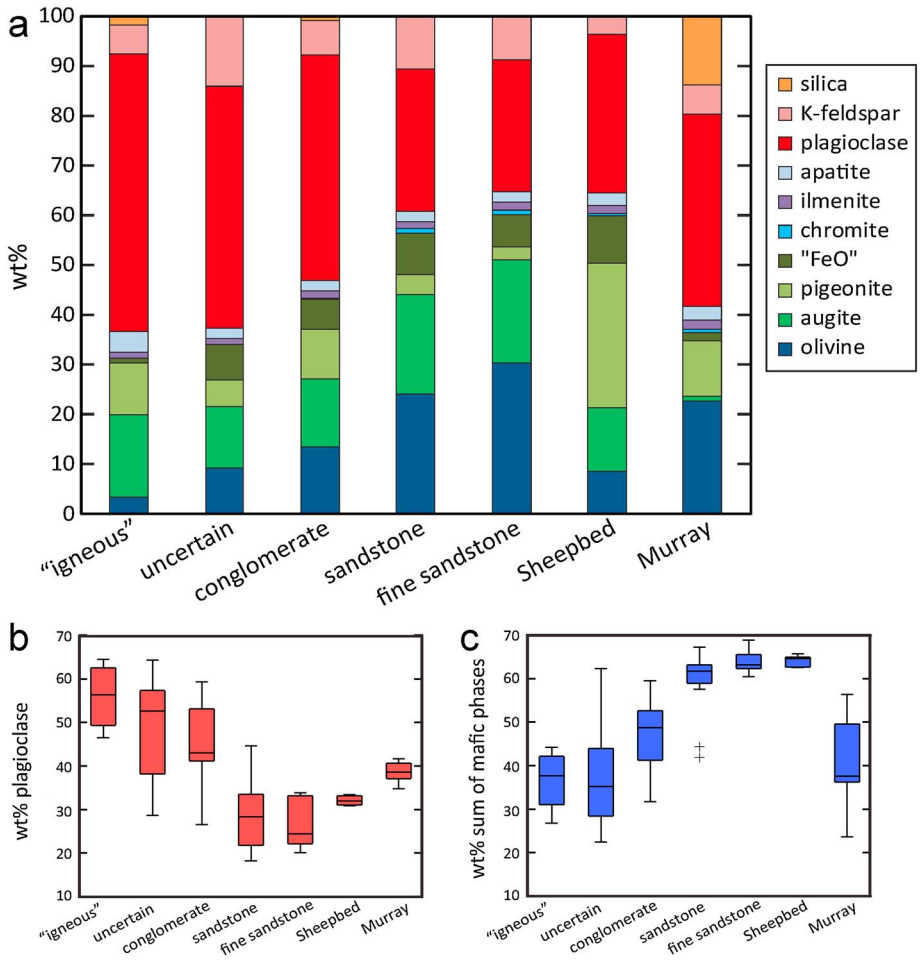

Figure 9. Diagrams showing the modeled mineralogy for each of the Bradbury group textural categories and Murray mudstone. (a) The mean weight percent of each mineral for each textural class. (b and c) Box plots, following the convention described in the caption of Figure 3, showing the range of plagioclase and mafic components within the textural classes. (c) The sum of mafic phases is the sum of olivine, pyroxenes, "FeO," chromite, and ilmenite.

synthetic Sheepbed composition decreases the calculated modal pyroxene ratio from ~2.3 to ~0.02 (calculated pigeonite abundance drops from ~30% to ~0.01%). The fact that the calculated modal abundances of pigeonite in the diagenetic targets range from 0 to 54% (Table S3 and supporting information) and do not correlate with bulk SO_3 suggests that $CaSO_4$ is not the sole source of sulfur in these rocks.

The mineralogical models for the Bradbury group APXS compositions allow mineral-based comparisons between the different textural classes. A bar chart showing the mean modeled mineralogy of each textural class is show in Figure 9a. This chart is consistent with the oxide-based models in Figures 6 and 7 and provides mineralogical context for the observed major- and minor-element variations in the Bradbury group rocks—as a function of grain size, the compositional differences reflect an increase in modal plagioclase and a decrease in the abundances of the mafic phases with increasing grain size (Figures 9b and 9c). Plagioclase content is quite high in the possible igneous and uncertain rock categories (averaging 56 and 47 wt %, respectively), slightly lower in the conglomerates (45 wt %), and substantially lower in sandstones and fine sandstones (29 and 27 wt %, respectively). The average of the calculated plagioclase modes for the Sheepbed mudstone targets is 32 wt %. We interpret the higher modal abundance of plagioclase in these nominally finer-grained rocks as reflecting a difference in the depositional environment between the fine Sheepbed mudstones and the coarser-grained rocks.

Another interesting difference between the Sheepbed mudstones and the other rocks comprising the Bradbury group is in the calculated modal abundance of pigeonite. The average pigeonite mode in the

mudstones is ~29 wt %, substantially higher than the average values for the other categories of rocks, 2.5–10 wt %. At first glance, this might suggest a larger contribution in the Sheepbed mudstones of detritus from subalkaline rocks than in the rocks from the other categories. However, as noted above, the presence of $CaSO_4$ in a bulk composition substantially lowers the calculated modal abundance of pigeonite. Calcium-sulfate veins are known to pervasively transect every unit *Curiosity* has explored, including the Bradbury group [*Nachon et al*., 2014], the Murray formation [*Grotzinger et al*., 2015; *Kah et al*., 2015; *Kroynak et al*., 2015], and Stimson formation [*Newsom et al*., 2016], so it seems assured that varying amounts of $CaSO_4$ are present in the analytical volume of every rock analyzed by APXS. Thus, our calculation may well underestimate the modal abundance of pigeonite in many of the unambiguously sedimentary rocks. This would imply a potential increase in the proportion of subalkaline relative to alkaline rocks that have supplied sediments to Gale crater.

5. Discussion

Any hypothesis for explaining the observed APXS compositional variations between Bradbury group targets must address variation from chemical weathering, source rock input, transport processes, and diagenetic cements. This study has shown that a meaningful hypothesis must also be constrained by the following observations:

1. Compositional variations among nondiagenetic Bradbury targets are nearly linear on element-element plots and are strongly correlated with grain size/textures of these sedimentary rocks (Figures 6 and 7).
2. This compositional variation is consistent with enrichment (in coarser-grained targets and float rocks) or depletion (in fine-grained rocks) of plagioclase minerals (Figures 6 and 9).
3. Bradbury rocks have extremely low CIA values (Figure 4), and 90% of the target compositions can be modeled using only primary igneous minerals (Figure 9).
4. Although, on average, potassium is inversely correlated with MgO (Figure 7h), elevated K_2O abundances are most strongly associated with stratigraphic position (Figure 5).

5.1. Chemical Weathering

The chemical weathering of igneous rocks involves chemical reactions that transform the high-temperature constituent minerals into new low-temperature secondary minerals. This commonly occurs during igneous rock breakdown and/or transport of the detrital fragments, where some chemical elements from mineral grains and/or glass may be removed from the system, typically by dissolution and fluid migration, causing changes in the bulk chemistry of the rock. Alternately, if chemical reactions occur after sediment deposition during diagenesis, they may occur in a closed system, where chemical breakdown of the minerals $\pm$ glass occurs but the chemical constituents remain, producing secondary minerals without changing the bulk chemistry of the sediment. Without a priori knowledge of the composition of sediment input, the extent to which weathering has occurred must be inferred by comparing the bulk compositions of a suite of rocks to compositional trends produced during terrestrial weathering of mafic and felsic rocks or experimental weathering of rocks under various pH conditions.

In this study, three methods are used to assess the degree of open-system chemical weathering: Chemical Index of Alteration (CIA) values, trends on the mafic ternary diagram, and mineralogical modeling to see if target compositions deviate from those expected from combinations of a set of igneous minerals. All three methods, described below, indicate that open-system chemical weathering in the Bradbury group rocks was minor.

Open-system chemical weathering in rocks on Earth and Mars is frequently quantified using the Chemical Index of Alteration (CIA), a molar ratio of Al_2O_3 over the sum of K_2O, CaO, Na_2O, and Al_2O_3 that serves as a proxy for the weathering of feldspars and Ca-bearing pyroxene (Figure 4a) [*Nesbitt and Young*, 1982, 1984; *Nesbitt*, 2003; *McLennan et al*., 2014]. In studies of terrestrial sedimentary rocks, CaO is corrected to only include calcium in silicate minerals (designated CaO*); since this is not well constrained on Mars, we do not apply such a correction here, and so reported CIA values are lower than they would be if corrected and should be considered minimum values. Fresh terrestrial mafic rocks have CIA values of ~30–45; shergottites have values that range from 19 to 41, with a majority between 28 and 40. For terrestrial rocks, values above ~45 may indicate some exposure to weathering, and values above ~50–55 are evidence for some

history of open-system chemical weathering [*McLennan et al*., 2014]. Since many of the sedimentary rocks in Aeolis Palus have broadly basaltic compositions, the first components to chemically weather are likely to be olivine and basaltic glass (if it is present). In a mafic ternary A-CNK-FM diagram, open-system chemical weathering of these two phases produces a trend in the residual material that parallels the red arrow in Figure 4b, i.e., the residues of open-system weathering plot above the feldspar-olivine join. Figure 4b shows that the nondiagenetic Bradbury group rocks all plot below this join.

The lack of open-system chemical weathering in the Yellowknife Bay formation, the lowest part of the Bradbury group, was first established by detailed measurements of the Sheepbed mudstone. Compositional data for this unit are very similar to average Mars crust [*Taylor and McLennan*, 2009] and have very low CIA values (up to 37.5), indicating that for the major oxides there was minimal open-system chemical weathering of these detrital rocks [*McLennan et al*., 2014]. However, CheMin X-ray diffraction data revealed that this unit is composed of 20–30% phyllosilicates, which are interpreted to be authigenic clays formed within the ancient lake that deposited the mudstone [*Grotzinger et al*., 2014; *Vaniman et al*., 2014]. These observations indicate that even where significant amounts of water were present and authigenesis occurred via the formation of secondary minerals, there is still a lack of evidence for significant open-system chemical weathering.

Analyses of coarser-grained Bradbury sediments also show a lack of evidence for open-system chemical weathering. Of the 112 rock analyses considered here, 10 have CIA values above 40, and all are below 45 (Figure 4a). No weathering trends appear on the mafic ternary diagram (Figure 4b). Additionally, 90% of all of the nondiagenetic rock compositions observed, including float rocks, can be modeled as a mixture of primary igneous minerals with a 95% confidence interval (Figure 9). This indicates that the compositional variability in 90% of the targets could merely reflect different mixtures of primary igneous minerals with reasonable Martian mineral compositions. There is very little evidence for any extensive open-system chemical weathering or cation loss from these sediments. Note that this trend does not continue into the Mount Sharp sediments, which show a more complex weathering history, resulting in CIA values of 37–53. Only four analyses of the Mount Sharp sediments have CIA <40, and 40% of the bulk compositions cannot be modeled by any combination of our set of primary igneous minerals (including silica).

Overall, since nearly all of the chemical variability among Bradbury group targets can be modeled as mixtures of primary igneous mineral grains, there is insufficient evidence to show that these targets have experienced open-system chemical weathering. We support the original interpretation of this trend by *McLennan et al*. [2014], who suggested that the climate was cold at the site of weathering along the crater rim—warm enough to allow liquid water to be stable and support overland flows [*Williams et al*., 2013; *Grotzinger et al*., 2014; *Szabó et al*., 2015] and the existence of long-lived lakes [*Grotzinger et al*., 2014; *Grotzinger et al*., 2015] but cool enough to severely limit the rates of chemical weathering.

5.2. Mechanisms for Potassium Variation

Perhaps the most distinctive elemental trend in the measured suite of Bradbury targets—potassium variation—is not correlated with grain size, at least for those rocks (conglomerates to mudstones) where we can unambiguously infer relative grain sizes (K_2O is enriched in rocks in the uncertain category relative to many of the conglomerates to mudstones). Potassium contents are strongly enriched in rocks that occur in a relatively narrow stratigraphic interval (Figure 5). As with other elements, potassium could be enriched by contribution of a distinctive source region enriched in potassium [*Treiman et al*., 2016], hydrodynamic sorting of potassic minerals during transport [*Nesbitt and Young*, 1996], or postdepositional chemical alteration such as potassium metasomatism [*Glazner*, 1988]. *Treiman et al*. [2016] discuss the source of the potassium in detail; we summarize key relevant arguments here.

Increased potassium due to hydrodynamic sorting of a potassium-rich phase such as alkali-feldspar or potassium metasomatism within the sediments in the Kimberley outcrop is inconsistent with the APXS and CheMin analyses. Potassium contents do not trend with grain size for our target set, unlike other elemental trends, indicating that density or grain size sorting does not dominate the potassium distribution at the scale of the Bradbury group. Chemically, the presence of easily altered olivine in the drilled target ("Windjana"), the lack of compositional trends in A-CN-K space indicative of the influx of K-rich fluids [*Fedo et al*., 1995], and the lack of any hydrothermal alteration minerals in the CheMin data [*Treiman et al*., 2016] suggest that

extensive open-system chemical weathering of the source rock or alteration in the Kimberley formation is not the cause of the observed K_2O enrichments. The trend in potassium content with stratigraphic height (Figure 5) makes it clear that potassium is highly concentrated in a relatively narrow sedimentary interval, which likely reflects detrital input from potassium-rich source rocks. The CheMin X-ray diffraction data on the Windjana target show that it contains significant amounts of pigeonite (11%) and sanidine (21%), which are unlikely to coexist in the same igneous rock (as noted by *Treiman et al*. [2016], a terrestrial example where they do coexist is the Fault Canyon flow [*Fuis*, 1996]; the rock contains ~56.7 wt % SiO_2, has a K_2O/Na_2O ratio of 3.5, and is subalkaline). Thus, based on mineralogy alone, igneous rocks representing either widely different potassium to sodium ratios (average K_2O/Na_2O for terrestrial subalkaline basalts are generally <0.4 [*Le Maitre*, 1976]), degrees of fractionation (e.g., basaltic to rhyolitic), and/or different rock series (e.g., subalkaline and alkaline) must have contributed detrital material to this target.

Investigation of the crystal chemistry of the mineral components based on the XRD analysis reveals further evidence that the potassium source is a distinctive detrital component. Based on unit-cell parameters, *Treiman et al*. [2016] inferred that the K-feldspar is ~Or_{95}. Such potassium-rich sanidine is rare in volcanic rocks [e.g., *Carmichael et al*., 1974]—alkali-feldspars in evolved undersaturated and saturated alkali-rich rocks are, when more potassic than anorthoclase, generally in the range $Or_{40–60}$ [e.g., *Carmichael*, 1965; *Henderson and Gibb*, 1983; *Nekvasil et al*., 2000]. (We note that CheMin estimates of alkali-feldspar compositions in the Murray rocks are more sodic and, in fact, much closer to the upper limit given above for alkali-rich terrestrial rocks (Rampe, personal communication), and thus, the Or_{95} composition may not be representative of K-feldspar-rich rocks in the Gale crater watershed.) Estimated average Mg#s of the olivine, augite, and pigeonite based on the Windjana XRD pattern are consistent with these three phases being in Fe-Mg equilibrium [*Treiman et al*., 2016]. Thus, the mafic phases may be from subalkaline rocks of roughly basaltic composition while the Or_{95} sanidine must be sourced from evolved alkaline rocks of unusual composition. Alternatively, given the large uncertainties on the estimated Mg#s, some fraction of the augite and olivine may also come from an alkaline source that may or may not be that which supplied the K-feldspar. For further details and petrologic implications, we refer the reader to *Treiman et al*. [2016].

Given the trends in Figure 5, it seems clear that the source rocks that contributed the sanidine were only supplying substantial amounts of this component at certain times during the filling of the Gale basin, which caused certain stratigraphic intervals, such as the Kimberley formation, to be strongly enriched in sediment from that source region, whereas other intervals were not significantly affected (although elevated K_2O throughout the unit implies that very minor amounts of this sediment source may have contributed throughout the stratigraphy). The characteristics of the sanidine, derived from CheMin, require that it was sourced from an unusual alkaline igneous rock, distinct from the source that supplied the majority of the Bradbury group sediment, so there must be at least two types of igneous source rocks within the watershed that supplied Bradbury group sediments. Without sufficiently high-resolution chemostratigraphic data collected across this part of the Bradbury group, it is not clear whether or not hydrodynamic sorting had any effect on potassium distributions within the Kimberley formation.

5.3. Major Influences on the Composition of the Bradbury Group

5.3.1. Source Rock Overview

The provenance of sedimentary rocks describes the collection of all rock types that were weathered and eroded to produce sediment that was transported and deposited in a sedimentary basin. Sedimentary provenance studies use the chemical composition, including isotopes, and the mineralogy, including detrital heavy minerals, of sedimentary rocks to infer the original source rock compositions and the effects of weathering processes that caused the source rocks to break down into sediment [e.g., *McLennan et al*., 2003; *Weltje and von Eynatten*, 2004]. For fluvial sediments, source rocks are typically the local rock units upstream in the watershed that are exposed to surface weathering [*Nesbitt et al*., 1996]. In contrast, eolian and lacustrine sediments commonly include material from more widespread sources because they can integrate rock fragments transported longer distances by the wind and/or sediments from all catchments around a basin. In terrestrial cases, the majority of sediment is derived from preexisting sediment (i.e., sediment recycling), which obscures identification of original igneous/metamorphic sources. The extent of sediment recycling is not well constrained for Mars, but it is not believed to play a significant role as it does on Earth [*McLennan and Grotzinger*, 2008]. Although sorting of grains during transport and later diagenetic processes

can obscure provenance, the initial size distributions of different mineral phases are controlled by the textures of the source rocks (e.g., volcanic versus plutonic), so the extent of sorting by grain size and density depends heavily on provenance [*Ohta*, 2004; *Fedo et al*., 2015].

The primary minerals that comprise the Bradbury group rocks were likely sourced from the Noachian terrain above the northern rim of the crater based on sediment transport directions and local geomorphic and stratigraphic features [*Palucis et al*., 2014; *Grotzinger et al*., 2015; *Szabó et al*., 2015]. Rocks within this region are known from orbital hyperspectral imagery to contain olivine [*Ehlmann and Buz*, 2015], but otherwise, there are relatively few constraints on the petrology of the rocks in the watershed. Thus, we do not know a priori what provenance signals may be expressed in the detritus that accumulated as the Bradbury group. However, the bulk compositions of the Bradbury group rocks provide some insight into the overall nature of the sediment source. With the exception of K_2O and Cl, the average major-element composition of the nondiagenetic Bradbury group rocks and average Martian soils (a proxy for average Martian crust [*Taylor and McLennan*, 2009]) overlap at 1 sigma. The average K_2O content of the Bradbury group rocks is more than a factor of 3 greater than that estimated for average Martian soils, consistent with indications that at least some of the igneous rocks in the region around Gale crater are more alkaline than might be inferred from Martian meteorites and are perhaps comparable to terrestrial alkali basalts and their derivative magmas [e.g., *Stolper et al*., 2013].

The characteristics of the igneous rocks supplying the minerals found in the Gale crater sediments can also be inferred from observations of large grains of definitively igneous rocks that occur as clasts in conglomerates. While *Curiosity* has observed several rocks with potentially igneous textures (and analyzed four of these with APXS), the most definitive igneous rock texture was observed with the Mastcam and ChemCam instruments at the Harrison target, in a large clast within a conglomerate ("Harrison" target), on sol 514 [*Sautter et al*., 2015; *Mangold et al*., 2016]. Harrison is composed of ~50% light-toned plagioclase phenocrysts set in a dark fine-grained matrix [*Sautter et al*., 2015]; if Harrison is representative of at least some of the source rocks contributing material to the Bradbury group, the sediments (prior to transport) may have contained larger grains of plagioclase and finer grains of mafic minerals. Texturally, several of the other clasts in conglomerates and "possible igneous" targets analyzed by APXS also appear to show large light-colored (plagioclase?) grains set in a dark matrix (mafic phases?). However, because the textures are ambiguous, the compositions of these clasts do not necessarily reflect primary igneous compositions—the clasts may be sedimentary, and the analyses include a contribution from dust. In the final section, we return to the issue of what the CheMin and modeled mineralogy of the Bradbury rocks imply about the compositions of their igneous sources.

The Murray mudstone, part of the Mount Sharp group, has at least a partially different provenance than the Bradbury group—the Murray mudstones have compositions that are distinct from all grain-size classes in the Bradbury group [*Gellert et al*., 2015; *Thompson et al*., 2015]. As a lacustrine deposit, the Murray mudstone, like the Sheepbed mudstone, may incorporate sediment from multiple watersheds and phases from authigenesis within the lake itself, so the provenance of the Bradbury group could also be a contributing source for the Murray mudstone. The elevated CIA values calculated for the bulk compositions of the Murray mudstones suggest input from some chemically weathered source regions, but the presence of apparently unaltered olivine and pyroxenes in the Murray formation indicates that the lake environment was not itself conducive to extensive mineral alteration (Figures 4a and 9). Some Murray sediments can be modeled as mixtures of primary igneous minerals if silica is included (Figure 9). The source of this silica could be as a phenocryst or groundmass phase from evolved igneous rocks in the watershed or from an authigenetic process. Other Murray sediments showed an excess in Al_2O_3 and/or P_2O_5 and a deficiency in Na_2O relative to the mass balance results, which may reflect a chemically weathered source region. Further investigation of the Murray mudstone is required to untangle the more complex factors involved in its formation, but it is sufficient for this study to recognize that the Murray unit has a more complex provenance than the Bradbury group, and should be treated independently.

5.3.2. Influence of Hydrodynamic Sorting

Sorting of sediment by density and grain size has long been recognized as an important process in the formation of sedimentary rocks [*Mackie*, 1923; *Weltje and von Eynatten*, 2004, and references therein], and sorting has also been observed in Martian sediments [*McGlynn et al*., 2012]. Early researchers noticed that within a natural sand target, heavy/dense minerals are concentrated in finer grain sizes and lighter minerals

are found in coarser grain sizes [*Rubey*, 1933; *Slingerland*, 1977]. Rubey modeled this phenomenon using Stokes' law to describe the settling velocity of particles with differing grain sizes and densities and showed that, for example, a spherical magnetite grain that is 0.63 mm in diameter is "hydrodynamically equivalent" to a spherical quartz grain 1.0 mm in diameter [*Rubey*, 1933; *Slingerland*, 1977]. While the shapes of minerals also play a role in mineral sorting by grain size, modern surveys show that equations based on hydrodynamic equivalence (i.e., particle settling velocities in a fluid) [e.g., *Ferguson and Church*, 2004] do quite well at describing the grain sizes of different minerals in a given mixed sediment target [*Whitmore et al*., 2004; *Garzanti et al*., 2008]. However, the minerals present and their size distributions in a given stream are dictated, at least initially, by the source region of the sediments, and thus, the provenance controls the availability of grains of a given hydrodynamic equivalence and, in turn, the presence or absence of downstream compositional trends [*Johnsson and Basu*, 1993].

The provenance of the Bradbury group is generally basaltic, and, based on visible grains in Harrison and the presence of mineral trends with grain size, at least some of the source rocks must have had plagioclase phenocrysts. The evidence described in this study indicates that chemical weathering does not play a major role here. Based on an analysis of grain roundness, *Szabó et al*. [2015] showed that the Gale crater sediments (at least those in conglomerates) have likely traveled on the order of ~50 km from their source, so Bradbury group sediments have traveled short distances relative to many sandstones on Earth. Sediments that reflect mechanical but not chemical weathering are difficult to find on Earth, but a few partial analogs are relevant.

In an effort to mimic the affects of mechanical weathering and impact-induced rock breakdown, *Fedo et al*. [2015] crushed and sieved two unweathered basalts: one porphyritic, from Kilauea, HI, and one aphanitic, from the Cima volcanic field, CA. They found that olivine and trace elements (Cr, Zn, and Ni) were concentrated in fine-grained fractions, while plagioclase was enriched in coarser-grained fractions, and that the compositional differences between sieved grain-size classes were greater for the porphyritic basalt. They pointed out that this compositional fractionation would be further enhanced by sorting during transport due to significant differences in grain size [*Fedo et al*., 2015]. *Nesbitt and Young* [1996] studied the bulk compositions of different grain-size sediments in a short (<5 km) glacio-fluvial system in Guys Bight Basin, where the bedrock is predominantly metamorphic gneisses, migmatites, and plutonic rocks composed predominantly of feldspars, quartz, biotite, and hornblende (the average bedrock composition is broadly "granitic"). The bedrock is comminuted by glacial processes and then sorted in a fluvial system, with low CIA values indicating minimal chemical weathering. Biotite and hornblende (and therefore FeO_T, TiO_2, and MgO) are concentrated in the muds and fine sands, whereas quartz and feldspar are relatively more abundant in medium and coarse sands [*Nesbitt and Young*, 1996], again following Bradbury group trends with mafic mineral enrichments in finer grain-size fractions and felsic mineral enrichments in coarser grain-size fractions.

The relative importance of the initial sizes of mineral grains (provenance) and the abrasion and breakdown of grains during transport in a fluvial system has been debated for Earth systems [e.g., *Ferguson et al*., 1996]. Overall, physical stresses tend to increase the number of monomineralic grains, thereby enhancing compositional variation with grain size by decreasing the number of lithic fragments [*Slatt and Eyles*, 1981]. Analysis of the particle shapes in Bradbury conglomerates indicates ~10–20% mass loss by physical abrasion [*Szabó et al*., 2015]. This suggests that if differential abrasion played a role in Bradbury sediment transport dynamics, it might have enhanced the number of monomineralic grains and the compositional grain-size signals related to provenance.

5.3.3. Influence of Diagenesis

The Bradbury group sedimentary rocks have clearly been lithified. There is evidence for burial of the Bradbury and Mount Sharp groups [*Schieber et al*., 2013; *Grotzinger et al*., 2015], so compaction likely played a role in lithification, but cementation was also an important part of the process. The timing of this lithification is constrained by late-stage calcium-sulfate-filled fractures, whose fluids do not appear to have pervasively penetrated into the surrounding rock—thus, the rocks must have been fairly well cemented prior to that fluid event [*Nachon et al*., 2014]. The lack of a clear chemical signal in the rock compositions that can be traced to enrichment of a cementing component makes it difficult to determine the composition of the cement, and it is possible that the cementing agent is distinct in different regions.

Iron oxide cement is likely in some, but not all, of the Bradbury group rocks. There are a limited number of float rocks analyzed by ChemCam [*Blaney et al*., 2014] and by APXS, (e.g., Et Then and Secure [*Schmidt*

et al., 2014]) that show persuasive evidence for iron oxide cements—each have >24 wt % FeO_T—but these are outliers compared to other targets. As discussed above, the majority of Bradbury group rocks have compositions that are consistent with primary igneous minerals; nevertheless, FeO is a phase in the mass balance, and its calculated modal abundance reflects the presence of igneous magnetite and/or Fe-rich cement (the mass fraction of FeO in the Bradbury targets ranges from 0 to ~0.16).

Cementation could also potentially be related to remineralization of the primary igneous grains that make up the rock targets. CheMin XRD analyses have shown that ~30% of each drilled target is amorphous [*Vaniman et al*., 2014; *Treiman et al*., 2016], and a detailed analysis of the amorphous component, incorporating uncertainties, indicates that it is not consistent with basaltic glass alone but is instead best approximated as a mixture of basaltic glass, hisingerite, amorphous sulfate, and nanophase iron oxides [*Dehouck et al*., 2014]. Additionally, significant phyllosilicates were present in CheMin XRD analyses of the Sheepbed member. Together, the mixed components within the amorphous material and the presence of phyllosilicates indicate that in situ alteration of the sediments occurred after deposition, and it is possible that the authigenic secondary minerals and amorphous material contributed significantly to the cementation of these rocks without altering the bulk composition at the scale of a given APXS analysis [*Dehouck et al*., 2014]. Compaction of phyllosilicates would help drive lithification, and salts or disordered minerals not only could help cement the rocks but also could become amorphous due to desiccation and thermal cycling in the harsh Martian climate, as described in *Vaniman et al*. [2004].

5.4. Bradbury Group Sediment Provenance

Based on the evidence presented in this study, the major-elemental variations of Bradbury rocks are consistent with plagioclase enrichment in the coarse-grained rock units and plagioclase depletion or mafic phase enrichment, in the fine-grained rock units (Figure 6 and section 4.6). The question then becomes what are the compositions of the rocks that supplied the plagioclase and mafic phases? Are all of these phases sourced from plagioclase-phyric basalts subjected to hydrodynamic sorting, or is the bulk of the plagioclase derived from more evolved compositions while the mafic phases (e.g., olivine, augite, and pigeonite) are sourced from basaltic compositions? Note that there may be a continuum between these two end-member scenarios. And finally, how volumetrically important are alkaline rocks as sources of detrital minerals to the Bradbury group sediments?

The dominant magmatic series in the Bradbury group provenance is revealed by the pyroxenes; the fact that refinements of the XRD patterns of the three targets analyzed by CheMin all yield significant mass fractions of pigeonite and that pigeonite is commonly present in the output of the mass balance calculations indicates that subalkaline basaltic rocks are an important source of sediments to Gale crater. Pigeonite is not a stable low-pressure crystallizing phase in alkaline magmas [e.g., *Wilkinson*, 1967; *Miyashiro*, 1978; *Sack et al*., 1987]. Olivine and augite are crystallizing phases in both subalkaline and alkaline magmas, and while there are compositional differences between augites that crystallize from these two magma series [e.g., *Kushiro*, 1960; *Deer et al*., 1978], CheMin cannot provide that detailed level of compositional information on the pyroxenes.

Previous work has suggested that basaltic shergottite-like compositions could be the source for the mafic phases within the Bradbury group [*Treiman et al*., 2016]. Indeed, pigeonite and augite are important phases in basaltic shergottites and olivine is a significant component of olivine-phyric shergottites [e.g., *Papike et al*., 2009; *McSween*, 2015]. However, while shergottite-like compositions could be the source for the mafic phases, Al_2O_3 contents in the shergottites are quite low relative to the bulk of terrestrial lavas (e.g., those on ocean islands; Figure 8), and thus, the amount of normative plagioclase in the shergottites is also low (24 ± 12 wt %, mean $\pm 1\sigma$, compared to 51 wt % for the average mid-ocean ridge basalt composition from *Gale et al*. [2013]). This means that plagioclase is unlikely to be an early crystallizing (i.e., phenocryst) phase in shergottite magmas, which in turn would rule out lavas with shergottite-like compositions as the source of the "large" plagioclase grains in the Bradbury group sedimentary rocks (NWA 2800 is a possible exception with 61 wt % normative plagioclase).

If shergottite-like compositions were sources for the mafic phases, then coarse plagioclase crystals would need to be contributed by another igneous source. CheMin alone cannot constrain the extent to which plagioclase may have been sourced from more basaltic or more evolved compositions (here we take the uncertainties in plagioclase An-values reported in *Treiman et al*. [2016] as being representative).

Nevertheless, silica-saturated and highly evolved subalkaline or transitional rocks (see *Nekvasil et al*. [2000] for a discussion) are unlikely to be major components of the source rocks that provided detrital grains to the Bradbury group. First-cycle terrestrial sediments sourced from continental areas (even those with abundant exposed basaltic terrains, e.g., Columbia River) generally contain substantial quartz [e.g., *Whetten et al*., 1969; *Palomares and Arribas*, 1993; *Nesbitt and Young*, 1996]. In contrast, only two of the Bradbury group rocks require silica in order to achieve an acceptable fit (Table S3). The fact that silica is not required in nearly all of the mass balance fits means that neither the source of the coarse plagioclase crystals nor the source of the K-feldspar is likely to be a highly evolved silica-rich magma (e.g., a rhyolite); such an evolved composition would most likely contain a free silica phase. Furthermore, as discussed in section 4.5, compositional trends based on incorporation of lithic fragments from more evolved rocks do not show the same slopes in FeO_T-MgO and Al_2O_3-MgO space as the Bradbury group compositional trends (Figure 8). Thus, the source of the coarse plagioclase was likely a subalkaline basalt, and the source of the sanidine was, in all likelihood, an alkaline rock.

The dominant provenance for the Bradbury sediments is most consistent with a subalkaline basalt that contains both significant early-crystallizing plagioclase and fine-grained mafic phases. *Rogers and Nekvasil* [2015] offer a mechanism whereby such plagioclase-rich liquid might be produced—the model involves ~50% fractionation of more typical Martian basaltic compositions at the base of the crust followed by eruption of residual liquids with ~48 wt % normative feldspar (assuming a relatively dry melt). Alternatively, relatively low degrees of partial melting (~5 to 12%) of a primitive Martian mantle composition at 1 GPa [*Collinet et al*., 2015] can produce basaltic melts with high normative plagioclase contents (66 to 55 wt %). Within the collection of Martian meteorites, examples of more plagioclase-rich rock types are seen in the bulk compositions of clasts in NWA 7533. These clasts are significantly more aluminous than the shergottites at the same MgO content (Figure 8), and have a mean normative plagioclase content of 39 ± 5 wt %, so rocks with compositions similar to these NWA 7533 clasts might be the source of the plagioclase grains in rocks of the Bradbury formation. We note that within these meteorite clasts, olivine appears to be extremely rare, and thus, if the NWA 7533 compositions are representative, olivines in the Bradbury group sediments would need to come from additional sources with more olivine-normative compositions, i.e., compositions more like the olivine-phyric shergottites.

Linear trend lines showing preferential plagioclase enrichment in coarse-grained materials and mafic enrichment in fine-grained materials are consistent with expected trends from communition and sorting during transport of the mechanical weathering products of plagioclase-phyric igneous rocks. Physical weathering of rocks breaks the rocks down into component mineral grains, which has been shown to concentrate the mafic minerals in the finest grain-size fraction and the less dense felsic grains in the coarser grain-size fraction when plagioclase grains occur as phenocrysts [*Fedo et al*., 2015]. During transport, the finest grains remain in suspension and compositional sorting is enhanced because the plagioclase grain sizes are so much larger than the mafic grain sizes that they are preferentially deposited upstream, in conglomerate facies, whereas the finer olivine and mafic grains remain in suspension until they are deposited downstream in fine-grained sandstones and lacustrine mudstones [*Nesbitt and Young*, 1996; *Whitmore et al*., 2004; *von Eynatten et al*., 2012]. This is consistent with the observation that the primary variations between targets are defined by their grain size and proportion of minerals. Furthermore, the enrichments in Cr_2O_3 in the finer grain-size rocks (Figure 6g) are consistent with enrichments in spinel, a phase that although dense, is generally very small relative to silicate phases (e.g., volume ratios of olivine to spinel in Hawaiian, Icelandic, and mid-ocean ridge basalts are ~100 to >1000, with spinels generally 10–50 μm in size [*Roeder*, 2006]). Sorting of igneous (largely basaltic?) mineral grains during communition and transport is the most consistent explanation for the major compositional trends in Bradbury group compositional data.

Deviations from the principal plagioclase enrichment trend in the Bradbury rocks are expected, given second-order variations in relative mineral abundances, dust cover, and extents of cementation. For example, late-stage diagenetic calcium-sulfate veins are prevalent and may partially decouple the concentrations of CaO (by APXS) from modal proportions of plagioclase and high-Ca pyroxene. *McLennan* [2000] discussed the issue of compositional deviations from primary mixing trends and showed how the addition of various sulfate and Fe- and Ti-rich phases could partially obscure the mixing relationships between rocks and soil at the Viking and Pathfinder sites. The finding that 90% of Bradbury rocks can be modeled as mixtures of

primary igneous phases implies that some deviations from the principal trends could merely represent uneven distributions of other primary minerals during breakdown and transport.

The compositions of the Sheepbed mudstones do not define the mafic end of the compositional spectrum of the Bradbury group rocks but tend to sit between the fine and coarse sandstones of the Bradbury group (Figures 6 and 7). The Sheepbed member is also the only nonfluvial, lacustrine mudstone targeted in the Bradbury group, so it has a much higher chance of incorporating sediment from eolian sources and other fluvial sources from around the crater, in addition to capturing the finest particles in the suspended load, which have a more mafic composition than the coarser grain-size deposits (Figures 6 and 7). Float rocks, especially those with obscured textural features, categorized here as uncertain, are also responsible for some of the largest deviations from the major compositional trends shown in Figure 3, make up a majority of the nondiagenetic Bradbury rocks that cannot be mass balanced using primary igneous minerals, and also display some of the largest deviations in the various oxide-MgO plots in Figures 6 and 7.

Finally, the potassium content of Bradbury group rocks is not directly related to the mineral sorting trends but instead reflects the presence of a distinctive minor source in the Gale crater watershed that is rich in sanidine. Mineralogical data at the Kimberley outcrop, with the highest concentration of potassium, show that the rock is still dominated by mafic minerals and more importantly contains pigeonite, a mineral indicative of a subalkaline source (as discussed above and in *Treiman et al*. [2016], whereas the source rock of the sanidine is most likely alkaline). The sanidine therefore is a mineralogic indicator of a distinctive source that contributes to at least one stratigraphic interval that is otherwise dominated by the main Bradbury group provenance.

6. Summary

Compositions of rocks from the Bradbury group in Gale crater offer a unique data set for sedimentary petrology because these rocks appear to have experienced minimal cation loss due to chemical weathering, the sedimentological context as a fluvio-lacustrine system is generally understood, and a variety of textures and grain sizes were targeted. Using this data set we can make inferences concerning the petrology of the source regions and the sedimentary processes that produced these rocks.

The principal geochemical trends for these targets reflect a concentration of plagioclase minerals in the coarsest-grained rocks and a concentration of mafic minerals in the finer-grained rocks. Investigation of the geochemical trends and Monte Carlo modeling of the bulk compositions in order to calculate mineral modes show that these trends are consistent with hydrodynamic segregation of plagioclase phenocrysts from mafic groundmass minerals during transport. In all likelihood, the dominant sources of these minerals were plagioclase-phyric subalkaline rocks of roughly basaltic composition. While the extent to which it is possible that plagioclase and some fraction of the mafic phases were derived from more or less evolved lavas is difficult to constrain, the apparent lack of silica in the vast majority of the Bradbury targets does suggest that highly evolved silica-rich compositions were, if present, rare.

The highly potassic sanidine in the Windjana target at the Kimberley outcrop [*Treiman et al*., 2016] is, by analogy with terrestrial examples, most likely sourced from highly alkaline rocks that only periodically contributed substantial sediment to the Gale crater basin; however, K_2O/Na_2O ratios in many of the Bradbury rocks are slightly above the value for average Martian crust, suggesting a near-continuous small sediment contribution from these highly alkaline rocks. Given the limited number of landed missions to Mars, and the relative paucity of basaltic sediments on Earth's continents, our analysis of the Bradbury group has provided a unique opportunity to understand the effects of provenance, weathering, transport, and cementation on a set of fluvial sedimentary rocks derived from largely basaltic sources.

Appendix A

A1. APXS

The Alpha Particle X-ray Spectrometer obtains bulk chemistry for a 1.5 cm diameter spot on in situ rock surfaces. When the APXS is deployed, the target is irradiated with energetic alpha particles and X-rays by the internal ^{244}Cm source. The X-rays emitted from the target are registered with a high-resolution silicon drift detector. The APXS method therefore resembles a combination of X-ray fluorescence and particle-induced X-ray emission. Lower *z* elements are predominantly excited by alpha particles and higher *z*

elements by the X-rays, with equal contributions around titanium. The penetration depth ranges from 2 to ~100 μm, increasing with elemental mass.

The X-ray spectra are converted into chemical concentrations using an MSL-adapted version of the empirical method described in *Gellert et al*. [2006]. The areas of the characteristic peaks of each element are determined with a nonlinear least squares fit algorithm, and the peak areas are then transformed into elemental concentrations using the extended calibration target set for MSL, comprising about 150 geological reference materials and additional simple chemical compounds. Accuracy errors are dependent on mineral characteristics; physics-based models assume a homogeneous, glass-like target to account for self-absorption of X-rays in the interpretation of the spectrum, which can be a poor assumption for compositionally heterogeneous mineral grains, particularly for low-*z* elements [*Gellert et al*., 2006; *Campbell et al*., 2012]. However, empirically, at the scale of the APXS measurement, diverse mixtures of different phases are assumed to largely overwhelm matrix effects associated with individual phases. Errors reported by the APXS team, and included here in Table S1, are statistical (2σ) errors based on the uncertainty of the peak areas. They represent precision (repeatability) errors, not accuracy errors, and they are correlated to factors like the measurement duration, standoff distance, and temperature as reflected in the spectrum fitting routine. See *Campbell et al*. [2012] for more details on the instrument calibration and estimates of analytical accuracy.

For each target, the sum of all oxides is normalized to 100% to compensate for variations in instrument standoff distance. The fact that the surface area analyzed by APXS is large relative to the mineral grains comprising the rocks in our data set suggests that the analyzed compositions (Table S1) reflect bulk surface compositions, and therefore, the APXS data are suitable for the investigations presented in this work. Given the variations in the depth of the analytical volume as a function of atomic number, trends in a data set that are based on elements with a range of *z* values will be of particular importance when such trends are used to support a particular model.

APXS targets are often analyzed under multiple conditions in order to obtain the maximum amount of information possible at a contact science stop with the rover for a particular target. The same target spot may be analyzed at multiple times of day in order to work around planning schedules. A raster across the rock may involve up to approximately five partially overlapping analyses on a heterogeneous rock surface in order to constrain the compositions of the observed heterogeneities (these overlapping spots are described as "offset" analyses). A target may be analyzed as is and then either analyzed with the ChemCam instrument (the shock front produced by the laser-induced breakdown spectroscopy technique frequently removes dust) or brushed with the dust removal tool (DRT) and then analyzed with the APXS instrument again with less dust cover. In some cases, a target was analyzed only after dust removal. If a target was drilled, the drill tailings adjacent to the hole were analyzed, as well as the discarded powder processed by sieving. For targets within the Bradbury group, 112 APXS analyses were completed on or offset from 73 distinct named rock targets. The DRT was only used on eight distinct named targets. For this study, in order to capture the variation between rock surface textures most completely, we include analyses both before and after dust removal as distinct analyses ("DRT" analyses; Table S1). In cases where the same unchanged target was analyzed at multiple times of day ("repeat" analyses; Table S1), we use only the analysis with the longest integration time (or optimal distance to target and/or thermal conditions), judged by the smallest reported statistical error associated with the measurement. Overlapping or offset analyses are included, because chemical variability can occur on short distance scales (offset analyses; Table S1). Drilled rock powders and soil targets were not included in order to only compare analyses on coherent rock surfaces.

APXS data are commonly normalized on a SO_3- and Cl-free basis in an effort to remove the effects of variable dust cover on the analyses [*Rieder et al*., 1997; *Schmidt et al*., 2014]. Sulfur is substantially enriched in Martian soil over what might be expected in a Martian basalt based on S analyses of SNC meteorites (5.2–8.9 wt % SO_3 [*Taylor and McLennan*, 2009] versus $<$0.01–0.7 wt % SO_3 [*Ding et al*., 2015]), and when analyses have been done on Martian surface rocks both before and after either brushing or abrading the surface, SO_3 and Cl abundances are uniformly lower in the latter analyses [*Rieder et al*., 2004; *Gellert et al*., 2006; *Ming et al*., 2008]. However, as discussed in *Stolper et al*. [2013], when analyses of both unbrushed and abraded surfaces of the same rock/outcrop [*Rieder et al*., 2004; *Gellert et al*., 2006; *Ming et al*., 2008] are compared on a SO_3- and Cl-free basis, the two sets of analyses are not substantially different (variations in SiO_2, Al_2O_3, FeO_T, MgO, and CaO are, on average, between 15 and 4%, relative). Importantly, this comparison included rocks with up to

~8 wt % SO_3 and ~1.3 wt % Cl, values that are comparable to those in the nondiagenetic targets in our data set (e.g., see sections 4.2 and 4.4). For this study, in the simple mixing calculations discussed in section 4.4, bulk rock compositions were not renormalized on a S- and Cl-free basis. For reasons that we discuss below in section A2, renormalized compositions were used in the Monte Carlo-based mass balance calculations. The fact that both sets of calculations yield the same first-order conclusions—that the compositional spectrum of a majority of the rocks that comprise the Bradbury group is consistent with substantial variations in the relative proportions of plagioclase versus olivine, augite, and pigeonite—also suggests that any other elements that are associated with S and Cl either in the dust or in veining material/cement have not substantially perturbed our analysis.

A2. Monte Carlo Mineralogy Model

As discussed briefly in section 4.6, weighted mass balance calculations were done using the bulk compositions of the Bradbury group rocks and the following set of phases: olivine, high- and low-Ca pyroxene, plagioclase, K-feldspar, apatite, ilmenite, chromite, iron oxide (as a proxy for magnetite), and silica. Although the details of the Monte Carlo mass balance calculation will be presented in a subsequent paper, here we discuss how the compositions of olivine, the pyroxenes, and the feldspars were constructed for each mass balance calculation (5,000,000 calculations were done for each bulk composition).

Cation abundances in olivines (Cr, Mn, Ca, and Ni) and pyroxenes (Ti, Al, Cr, Mn, Ca, Na, and Ni) from Martian meteorites (see section 4.6.1 for the main data sources) were related to Mg# [Mg/(Mg + Fe), molar] variations in each phase (e.g., olivine Mn versus olivine Mg# is well described by a polynomial), and for each calculation, a randomly selected Mg# was drawn from the range of Mg#s constrained by CheMin results on Gale crater samples. This Mg# determined the Cr, Mn, Ca, Ni, Fe, and Mg abundances in the olivine, and Si was fixed by stoichiometry. For some elements, e.g., Ca in the pyroxenes, the correlation between the cation and Mg# was poor, and in those cases, smooth lower and upper bounds (generally polynomials) were fit "by eye" to the meteorite mineral data in cation versus Mg# space, and a random number (with a flat distribution) was used in addition to an Mg# to select a cation value (see *Baker and Beckett* [1999] for further information on the stoichiometric constraints used to calculate pyroxene compositions). For plagioclase- and Ca-free alkali-feldspar, molar Ca/(Na + Na), Ca#, and K/(K + Na), K#, uniquely define the composition of each phase, and the bounds on these molar ratios were constrained by data from Martian meteorites and CheMin (Ca#) and CheMin (K#), respectively. We note that the alkaline nature of some of the rocks at Gale crater [e.g., *Stolper et al*., 2013; *Schmidt et al*., 2014; *Sautter et al*., 2015] suggests that the pyroxenes in these rocks may differ from those found in the SNC meteorites (pyroxenes in terrestrial alkaline rocks tend to be richer in Ti, Al, and Na compared to pyroxenes in subalkaline rocks [*Kushiro*, 1960; *Deer et al*., 1978]). However, pyroxene analyses from clasts in the polymict breccia, NWA 7034 and 7475 [*Santos et al*., 2015; *Wittmann et al*., 2015; *Nyquist et al*., 2016] inferred to be a sample of the early Martian crust [*Humayun et al*., 2013], constitute ~28% of our data set; some of these clasts are alkaline based on their bulk composition, and as we show in section 4.6.2, the majority of the mass balance calculations yielded extremely small residuals, indicating that Martian meteorite phase compositions can successfully be used to mass balance the compositions of Gale crater sedimentary rocks.

For each APXS bulk composition (Table S1), the reported mineral phase assemblage and proportions (Table S3) were calculated by averaging the output of 25 runs from the mass balance model, where a run consisted of 200,000 calculations and the best fit calculation for each run was the calculation with the lowest χ^2 value. Each best fit mass balance output for a given run was only deemed statistically acceptable if the *Q* value [e.g., *Press et al*., 1992] was $\geq$0.05 (i.e., acceptable at the 95% confidence level). The results from repeated runs on the same bulk composition showed that the sum of olivine plus the pyroxenes (augite and pigeonite) were not significantly variable from run to run, but the calculated individual fractions of these three mafic phases could vary well outside the range of their standard errors (even with no statistically significant difference in the χ^2 values). This variability in modal proportions of the major mafic silicate phases reflects the fact that although each individual mass balance calculation is overdetermined, the Mg# bounds on olivine and the pyroxenes are relatively loose; the range of potential Ca contents in the pyroxenes is large (e.g., from Wo_{21} to $Wo_{40.5}$ for augite); iron oxide (i.e., FeO_T) is a separate phase in the mass balance; and the bulk concentrations of four oxides, SiO_2, FeO, MgO, and CaO, are the most important in constraining the proportions of the three mafic silicate phases. Therefore, proportions of individual mineral phases for each of the Gale crater

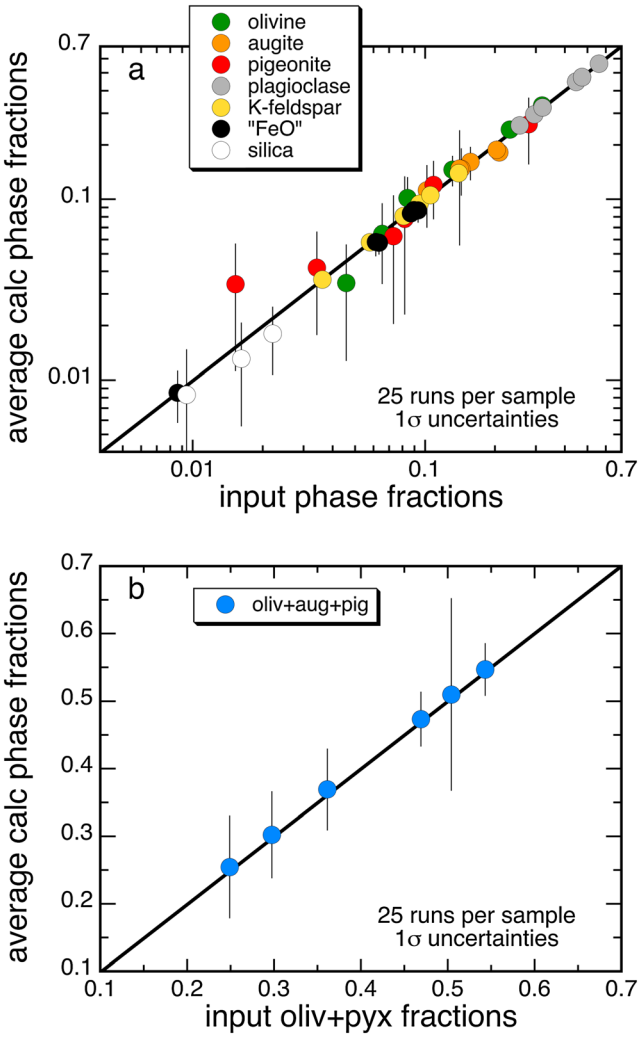

Figure A1. Comparison between input phase fractions and calculated phase fractions. The input phase fractions were used to generate six synthetic compositions (see Table S2) based on the six categories discussed in the main text. These six compositions were treated as unknowns, and their phase proportions were calculated using the mass balance routine described in the text. Each run consists of 200,000 mass balance calculations; for each run, the fit with the lowest χ^2 value is output and the 25 best fit phase fractions were averaged (see Table S2).

targets were determined by averaging the output from 25 runs. When the mass balance routine was used with the same parameters on synthetic bulk compositions constructed using average sets of phase proportions from the Bradbury group textural categories, again averaging the results from 25 model runs, calculated phase fractions overlapped within 1 standard deviation of the input phase fractions (Figure A1). Furthermore, Figure A1b shows that input and calculated olivine + augite + pigeonite fractions lie on the 1:1 line for each of the six bulk compositions (bulk compositions, input phase proportions, and calculated phase fractions are reported in Table S2). Averages of 50 runs (each run consisting of 200,000 calculations) for each of these 6 synthetic compositions are the same within error as those based on 25 runs.

The low-Ca pyroxene in our calculations was pigeonite. Based on Rietveld refinements of CheMin data [*Vaniman et al.*, 2014; *Morrison et al.*, 2015; *Treiman et al.*, 2016], pigeonite appears to be substantially more abundant than orthopyroxene in Gale crater rocks, and including three pyroxenes in the mass balance calculations leads to a linear degeneracy. Nevertheless, even with only two pyroxenes, some mass balance calculations returned negative mass fractions of olivine and/or pyroxene; after every individual calculation in a run of 200,000, any negative coefficients were set to zero and the mass balance calculation was repeated using the same phase compositions. The phase proportions were not constrained to sum to 1—as we discussed in section 4.6.2, the fact that all successful mass balance calculations yielded phase fraction sums very close to 1 suggests that our selection of minerals represents a self-consistent set of phases.

As noted above, bulk APXS compositions were renormalized on a S- and Cl-free basis. Although this may introduce a systematic bias (we discuss in Appendix A1 why we think that such a bias, if it exists, would not be large), initial calculations that included anhydrite and halite resulted in best fit plagioclase compositions that tended to be extremely albitic, i.e., with molar Ca/(Ca + Na) ratios of 0.1 to 0.2—substantially more sodic than plagioclase compositions estimated by CheMin [*Vaniman et al.*, 2014; *Morrison et al.*, 2015; *Treiman et al.*, 2016] even considering the fact that the calculated plagioclase compositions will tend to be more sodic then those estimated by CheMin if the sediment consisted of detrital plagioclase grains and fragments of Na_2O-rich groundmass. This suggests that although CaO and SO_3 are positively correlated in the APXS data set, some fraction of the sulfur is incorporated in noncalcium-bearing phases. The fact that we have only mass

balanced rocks that contain <12 wt % SO_3 limits the leverage that the renormalization exerts on the remaining oxides in these bulk compositions (indeed, none of the nondiagenetic Bradbury group rocks that were mass balanced contained more than ~8.5 wt % SO_3).

Acknowledgments
The authors are indebted to the MSL science, engineering, and management teams for their efforts in tactical and strategic operations and in enabling efficient operation of the rover. Without the support of these teams, the data presented here could not have been collected. The authors are also grateful to the science team for the helpful discussions and especially to N. Mangold and M. Schmidt for their helpful feedback on an earlier version of the manuscript. Insightful and constructive reviews by C. Fedo and J. Catalano further improved this manuscript. Some of this research was carried out at the Jet Propulsion Laboratory, California Institute of Technology, under a contract with NASA. The work was also partially supported by the NASA Astrobiology Institute. Data presented in this paper are archived in the Planetary Data System (pds.nasa.gov).

References

Ablay, G. J., G. G. J. Ernst, J. Marti, and R. S. J. Sparks (1995), The ~2 ka subplinian eruption of Montaña Blanca, Tenerife, *B Volcanol*, *57*(5), 337–355, doi:10.1007/bf00301292.

Anderson, R. B., and J. F. Bell (2010), Geologic mapping and characterization of Gale crater and implications for its potential as a Mars Science Laboratory landing site, *Mars J.*, *5*, 76–128, doi:10.1555/mars.2010.0004.

Andújar, J., and B. Scaillet (2012), Relationships between pre-eruptive conditions and eruptive styles of phonolite–trachyte magmas, *Lithos*, *152*, 122–131, doi:10.1016/j.lithos.2012.05.009.

Andújar, J., F. Costa, and J. Martí (2010), Magma storage conditions of the last eruption of Teide volcano (Canary Islands, Spain), *B Volcanol*, *72*(4), 381–395, doi:10.1007/s00445-009-0325-3.

Baker, M. B., and J. R. Beckett (1999), The origin of abyssal peridotites: A reinterpretation of constraints based on primary bulk compositions, *Earth Planet. Sci. Lett.*, *171*(1), 49–61, doi:10.1016/S0012-821x(99)00130-2.

Berger, J. A., et al. (2016), A global Mars dust composition refined by the Alpha-Particle X-ray Spectrometer in Gale crater, *Geophys. Res. Lett.*, *43*, 67–75, doi:10.1002/2015gl066675.

Blaney, D. L., et al. (2014), Chemistry and texture of the rocks at Rocknest, Gale crater: Evidence for sedimentary origin and diagenetic alteration, *J. Geophys. Res. Planets*, *119*, 2109–2131, doi:10.1002/2013je004590.

Bryan, W. B., L. W. Finger, and F. Chayes (1969), Estimating proportions in petrographic mixing equations by least-squares approximation, *Science*, *163*(3870), 926–927, doi:10.1126/science.163.3870.926.

Campbell, J. L., G. M. Perrett, R. Gellert, S. M. Andrushenko, N. I. Boyd, J. A. Maxwell, P. L. King, and C. D. M. Schofield (2012), Calibration of the Mars Science Laboratory Alpha Particle X-ray Spectrometer, *Space Sci. Rev.*, *170*(1–4), 319–340, doi:10.1007/s11214-012-9873-5.

Carmichael, I. S. E. (1965), Trachytes and their feldspar phenocrysts, *Mineral. Mag.*, *34*(268), 107–125, doi:10.1180/minmag.1965.034.268.09.

Carmichael, I. S. E., F. J. Turner, and J. Verhoogen (1974), *Igneous Petrology*, pp. 739, McGraw-Hill, New York.

Chesworth, W., J. Dejou, and P. Larroque (1981), The weathering of basalt and relative mobilities of the major elements at Belbex, France, *Geochim. Cosmochim. Acta*, *45*(7), 1235–1243, doi:10.1016/0016-7037(81)90147-2.

Cohen, D., and C. R. Ward (1991), SEDNORM—A program to calculate a normative mineralogy for sedimentary-rocks based on chemical analyses, *Comput. Geosci.*, *17*(9), 1235–1253, doi:10.1016/0098-3004(91)90026-A.

Collinet, M., E. Médard, B. Charlier, J. Vander Auwera, and T. L. Grove (2015), Melting of the primitive Martian mantle at 0.5–2.2 GPa and the origin of basalts and alkaline rocks on Mars, *Earth Planet. Sci. Lett.*, *427*, 83–94, doi:10.1016/j.epsl.2015.06.056.

Cox, R., and D. R. Lowe (1995), A conceptual review of regional-scale controls on the composition of clastic sediment and the co-evolution of continental blocks and their sedimentary cover, *J. Sediment. Res.*, *A65*(1), 1–12.

Deer, W. A., R. A. Howie, and J. Zussman (1978), *Rock-Forming Minerals*, *Single-Chain Silicates 2A*, 2nd ed., John Wiley & Sons, New York.

Dehouck, E., S. M. McLennan, P. Y. Meslin, and A. Cousin (2014), Constraints on abundance, composition, and nature of X-ray amorphous components of soils and rocks at Gale crater, Mars, *J. Geophys. Res. Planets*, *119*, 2640–2657, doi:10.1002/2014je004716.

Ding, S., R. Dasgupta, C.-T. A. Lee, and M. Wadhwa (2015), New bulk sulfur measurements of Martian meteorites and modeling the fate of sulfur during melting and crystallization—Implications for sulfur transfer from Martian mantle to crust–atmosphere system, *Earth Planet. Sci. Lett.*, *409*, 157–167, doi:10.1016/j.epsl.2014.10.046.

Edgett, K. S., et al. (2012), Curiosity's Mars Hand Lens Imager (MAHLI) investigation, *Space Sci. Rev.*, *170*(1–4), 259–317, doi:10.1007/s11214-012-9910-4.

Ehlmann, B. L., and J. Buz (2015), Mineralogy and fluvial history of the watersheds of Gale, Knobel, and Sharp craters: A regional context for the Mars Science Laboratory Curiosity's exploration, *Geophys. Res. Lett.*, *42*, 264–273, doi:10.1002/2014gl062553.

Engel, A. E., S. P. Itson, C. G. Engel, D. M. Stickney, and E. J. Cray (1974), Crustal evolution and global tectonics: A petrogenic view, *Geol. Soc. Am. Bull.*, *85*, 842–858.

Farley, K. A., et al. (2014), In situ radiometric and exposure age dating of the Martian surface, *Science*, *343*(6169), doi:10.1126/science.1247166.

Fedo, C. M., H. W. Nesbitt, and G. M. Young (1995), Unraveling the effects of potassium metasomatism in sedimentary-rocks and paleosols, with implications for paleoweathering conditions and provenance, *Geology*, *23*(10), 921–924, doi:10.1130/0091-7613(1995)023<0921:Uteopm>2.3.Co;2.

Fedo, C. M., G. M. Grant, and H. W. Nesbitt (1997), Paleoclimatic control on the composition of the Paleoproterozoic Serpent Formation, Huronian Supergroup, Canada: A greenhouse to icehouse transition, *Precambrian Res.*, *86*(3–4), 201–223, doi:10.1016/S0301-9268(97)00049-1.

Fedo, C. M., I. O. McGlynn, and H. Y. McSween (2015), Grain size and hydrodynamic sorting controls on the composition of basaltic sediments: Implications for interpreting Martian soils, *Earth Planet. Sci. Lett.*, *423*, 67–77, doi:10.1016/j.epsl.2015.03.052.

Ferguson, R. I., and M. Church (2004), A simple universal equation for grain settling velocity, *J. Sediment. Res.*, *74*(6), 933–937.

Ferguson, R., T. Hoey, S. Wathen, and A. Werritty (1996), Field evidence for rapid downstream fining of river gravels through selective transport, *Geology*, *24*(2), 179–182, doi:10.1130/0091-7613(1996)024<0179:Fefrdf>2.3.Co;2.

Filiberto, J. (2008), Similarities between the shergottites and terrestrial ferropicrites, *Icarus*, *197*(1), 52–59, doi:10.1016/j.icarus.2008.04.016.

Frihy, O. E., M. F. Lotfy, and P. D. Komar (1995), Spatial variations in heavy minerals and patterns of sediment sorting along the Nile Delta, Egypt, *Sediment. Geol.*, *97*(1–2), 33–41, doi:10.1016/0037-0738(94)00135-H.

Fuis, G. S. (1996), The geology and mechanics of formation of the Fort Rock Dome, Yavapai county, Arizona. USGS Professional Paper, 1266, pp. 95.

Gale, A., C. A. Dalton, C. H. Langmuir, Y. Su, and J.-G. Schilling (2013), The mean composition of ocean ridge basalts, *Geochem. Geophys. Geosyst.*, *14*, 489–518, doi:10.1029/2012gc004334.

Garrels, R. M., and F. T. Mackenzie (1971), *Evolution of Sedimentary Rocks*, pp. 397 , W. W. Norton & Company, New York.

Garzanti, E., S. Andò, and G. Vezzoli (2008), Settling equivalence of detrital minerals and grain-size dependence of sediment composition, *Earth Planet. Sci. Lett.*, *273*(1–2), 138–151, doi:10.1016/j.epsl.2008.06.020.

Gast, P. W. (1968), Trace element fractionation and the origin of tholeiitic and alkaline magma types, *Geochim. Cosmochim. Acta*, *32*, 1057–1086.

Gellert, R., and B. C. Clark (2015), In situ compositional measurements of rocks and soils with the Alpha Particle X-ray Spectrometer on NASA's Mars rovers, *Elements*, *11*(1), 39–44, doi:10.2113/gselements.11.1.39.

Gellert, R., J. L. Campbell, P. L. King, L. A. Leshin, G. W. Lugmair, J. G. Spray, S. W. Squyres, and A. S. Yen (2009), The Alpha Particle X-ray Spectrometer (APXS) for the Mars Science Laboratory (MSL) rover mission, presented at *40th Lunar and Planetary Science Conference*, Abstract 2364, LPI, Houston, Tex.

Gellert, R., et al. (2006), Alpha Particle X-Ray Spectrometer (APXS): Results from Gusev crater and calibration report, *J. Geophys. Res.*, *111*, E02S05, doi:10.1029/2005JE002555.

Gellert, R., et al. (2015), Chemical evidence for an aqueous history at Pahrump, Gale crater, Mars, as seen by the APXS, presented at *46th Lunar and Planetary Science Conference*, Abtract 1855, LPI, Houston, Tex.

Glazner, A. F. (1988), Stratigraphy, structure, and potassic alteration of Miocene volcanic rocks in the Sleeping Beauty area, central Mojave desert, California, *Geol. Soc. Am. Bull.*, *100*, 424–435.

Gross, J., A. H. Treiman, J. Filiberto, and C. D. K. Herd (2011), Primitive olivine-phyric shergottite NWA 5789: Petrography, mineral chemistry, and cooling history imply a magma similar to Yamato-980459, *Meteorit. Planet. Sci.*, doi:10.1111/j.1945-5100.2010.01152.x.

Grotzinger, J. P., et al. (2015), Deposition, exhumation, and paleoclimate of an ancient lake deposit, Gale crater, Mars, *Science*, *350*(6257), aac7575, doi:10.1126/science.aac7575.

Grotzinger, J. P., et al. (2014), A habitable fluvio-lacustrine environment at Yellowknife Bay, Gale crater, Mars, *Science*, *343*(6169), 1,242,777, doi:10.1126/science.1242777.

Henderson, C. M. B., and F. G. F. Gibb (1983), Felsic mineral crystallization trends in differentiating alkaline basic magmas, *Contrib. Mineral. Petrol.*, *84*, 355–364.

Hughes, M. G., J. B. Keene, and R. G. Joseph (2000), Hydraulic sorting of heavy-mineral grains by swash on a medium-sand beach, *J. Sediment. Res.*, *70*(5), 994–1004, doi:10.1306/112599700994.

Humayun, M., et al. (2013), Origin and age of the earliest Martian crust from meteorite NWA 7533, *Nature*, *503*(7477), 513–516, doi:10.1038/nature12764.

Iacovino, K., C. Oppenheimer, B. Scaillet, and P. Kyle (2016), Storage and evolution of mafic and intermediate alkaline magmas beneath Ross Island, Antarctica, *J. Petrol.*, *57*(1), 93–118, doi:10.1093/petrology/egv083.

Johnsson, M. J., and A. Basu (1993), Processes controlling the composition of clastic sediments, *Geol. Soc. Am. Spec. Pap.*, *284*, vii–viii.

Kah, L. C., R. E. Kroynak, D. W. Ming, J. P. Grotzinger, J. Schieber, D. Sumner, and K. Edgett (2015), Diagenetic crystal growth in the Murray Formation, Gale crater, Mars, presented at *Geological Society of America Annual Conference*, vol. 47, p. 267, Baltimore, Md.

Kelsey, C. H. (1965), Calculation of the C.T.P.W. norm, *Mineral. Mag.*, *34*, 276–282.

Komar, P. D. (2007), The entrainment, transport, and sorting of heavy minerals by waves and currents, in *Heavy Minerals in Use*, edited by M. T. Mange and D. T. Wright, pp. 3–48, Elsevier, Italy.

Kroynak, R. E., L. C. Kah, J. P. Grotzinger, M. Fisk, D. Sumner, M. Nachon, N. Mangold, D. Blaney, W. Rapin, and R. Wiens (2015), Garden City: A complex vein system observed by the Curiosity rover at Pahrump Hills, Gale crater, Mars, presented at *Geological Society of America Annual Conference*, vol. 47, p. 217, Baltimore, Md.

Kushiro, I. (1960), Si-Al relation in clinopyroxenes from igneous rocks, *Am. J. Sci.*, *258*(8), 548–554.

Lanza, N. L., et al. (2016), Oxidation of manganese in an ancient aquifer, Kimberley formation, Gale crater, Mars, *Geophys. Res. Lett.*, *43*, 7398–7407, doi:10.1002/2016gl069109.

Laube, N., S. Hergarten, and H. J. Neugebauer (1996), MODUSCALC—A computer program to calculate a mode from a geochemical rock analysis, *Comput. Geosci.*, *22*(6), 631–637, doi:10.1016/0098-3004(95)00127-1.

Le Deit, L., et al. (2016), The potassic sedimentary rocks in Gale crater, Mars, as seen by ChemCam on board Curiosity, *J. Geophys. Res. Planets*, *121*, 784–804, doi:10.1002/2015je004987.

Le Maitre, R. W. (1976), The chemical variability of some common igneous rocks, *J. Petrol.*, *17*, 589–637.

Léveillé, R. J., et al. (2014), Chemistry of fracture-filling raised ridges in Yellowknife Bay, Gale crater: Window into past aqueous activity and habitability on Mars, *J. Geophys. Res. Planets*, *119*, 2398–2415, doi:10.1002/2014JE004620.

Mackie, W. (1923), The principles that regulate the distribution of particles of heavy minerals in sedimentary rocks, as illustrated by the sandstones of the north-east of Scotland, *Trans. Edinburgh Geol. Soc.*, *11*, 138–164.

Malin, M. C., and K. S. Edgett (2000), Sedimentary rocks of early Mars, *Science*, *290*(5498), 1927–1937, doi:10.1126/science.290.5498.1927.

Mangold, N., D. Baratoux, O. Arnalds, J. M. Bardintzeff, B. Platevoet, M. Grégoire, and P. Pinet (2011), Segregation of olivine grains in volcanic sands in Iceland and implications for Mars, *Earth Planet. Sci. Lett.*, *310*(3–4), 233–243, doi:10.1016/j.epsl.2011.07.025.

Mangold, N., et al. (2016), Composition of conglomerates analyzed by the Curiosity rover: Implications for Gale crater crust and sediment sources, *J. Geophys. Res. Planets*, *121*, 353–387, doi:10.1002/2015JE004977.

Mangold, N., et al. (2017), Classification scheme for sedimentary and igneous rocks in Gale crater, Mars, *Icarus*, *284*, 1–17, doi:10.1016/j.icarus.2016.11.005.

Marsaglia, K. M. (1993), Basaltic island sand provenance, in *Processes Controlling the Composition of Clastic Sediments*, *Geological Society of America Bulletin, Special Paper*, vol. 284, edited by M. J. Johnsson and A. Basu, pp. 41–65, Boulder, Colo.

McGlynn, I. O., C. M. Fedo, and H. Y. McSween (2012), Soil mineralogy at the Mars exploration rover landing sites: An assessment of the competing roles of physical sorting and chemical weathering, *J. Geophys. Res.*, *117*, E01006, doi:10.1029/2011JE003861.

McLennan, S., and J. Grotzinger (2008), The sedimentary rock cycle of Mars, *Martian Surf.-Compos., Mineral.,Phys. Prop.*, *1*, 541.

McLennan, S. M. (2000), Chemical composition of Martian soil and rocks: Complex mixing and sedimentary transport, *Geophys. Res. Lett.*, *27*, 1335–1338, doi:10.1029/1999GL008432.

McLennan, S. M., B. Bock, S. R. Hemming, J. A. Hurowitz, S. M. Lev, and D. K. McDaniel (2003), The roles of provenance and sedimentary processes in the geochemistry of sedimentary rocks, in *Geochemistry of Sediments and Sedimentary Rocks: Evolutionary Considerations to Mineral Deposit-Forming Environments*, edited by D. R. Lentz, pp. 7–38, Geological Association of Canada: GeoText, St. Johns.

McLennan, S. M., et al. (2014), Elemental geochemistry of sedimentary rocks at Yellowknife Bay, Gale crater, Mars, *Science*, *343*(6169), doi:10.1126/science.1244734.

McLennan, S. M., E. Dehouck, J. P. Grotzinger, J. A. Hurowitz, N. Mangold, and K. Siebach (2015), Geochemical record of open-system chemical weathering at Gale crater and implications for paleoclimates on Mars, presented at *46th Lunar and Planetary Science Conference*, Abstract 2533, LPI, Houston, Tex.

McSween, H. Y. (2015), Petrology on Mars, *Am. Mineral.*, *100*(11–12), 2380–2395, doi:10.2138/am-2015-5257.

McSween, H. Y., and S. M. McLennan (2014), 2.10 - Mars, in *Treatise on Geochemistry*, edited by H. Holland and K. Turekian, pp. 251–300, Elsevier, Waltham, Mass.

McSween, H. Y., I. O. McGlynn, and A. D. Rogers (2010), Determining the modal mineralogy of Martian soils, *J. Geophys. Res.*, *115*, E00F12, doi:10.1029/2010JE003582.

Meyer, C. (2015), Martian Meteorite Compendium. [Available from: http://www-curator.jsc.nasa.gov/antmet/mmc/index.cfm (Accessed 2015).]
Miliragovic, D., and D. Francis (2016), Ca. 2.7 Ga ferropicritic magmatism: A record of Fe-rich heterogeneities during Neoarchean global mantle melting, *Geochim. Cosmochim. Acta*, *185*, 44–63, doi:10.1016/j.gca.2015.09.023.
Milliken, R. E., J. P. Grotzinger, and B. J. Thomson (2010), Paleoclimate of Mars as captured by the stratigraphic record in Gale crater, *Geophys. Res. Lett.*, *37*, L04201, doi:10.1029/2009GL041870.
Ming, D. W., et al. (2008), Geochemical properties of rocks and soils in Gusev Crater, Mars: Results of the Alpha Particle X-Ray Spectrometer from Cumberland Ridge to Home Plate, *J. Geophys. Res.*, *113*, E12S39, doi:10.1029/2008JE003195.
Miyashiro, A. (1978), Nature of alkali volcanic rock series, *Contrib. Mineral. Petrol.*, *66*, 91–104.
Morrison, S. M., et al. (2015), Crystal-chemical analysis of Martian minerals in Gale crater, presented at *46th Lunar and Planetary Science Conference*, Abstract 2506, LPI, Houston, Tex.
Moussallam, Y., C. Oppenheimer, B. Scaillet, and P. R. Kyle (2013), Experimental phase-equilibrium constraints on the phonolite magmatic system of Erebus Volcano, Antarctica, *J. Petrol.*, *54*(7), 1285–1307, doi:10.1093/petrology/egt012.
Nachon, M., et al. (2014), Calcium sulfate veins characterized by ChemCam/Curiosity at Gale crater, Mars, *J. Geophys. Res. Planets*, *119*, 1991–2016, doi:10.1002/2013JE004588.
Nekvasil, H., A. Simon, and D. H. Lindsley (2000), Crystal fractionation and the evolution of intra-plate hy-normative igneous suites: Insights from their feldspars, *J. Petrol.*, *41*(12), 1743–1757.
Nesbitt, H. W. (2003), Petrogenesis of siliciclastic sediments and sedimentary rocks, in *Geochemistry of Sediments and Sedimentary Rocks: Evolutionary Considerations to Mineral Deposit-Forming Environments*, edited by D. R. Lentz, pp. 39–51, Geological Association of Canada, Canada.
Nesbitt, H. W., and G. M. Young (1982), Early proterozoic climates and plate motions inferred from major element chemistry of lutites, *Nature*, *299*(5885), 715–717, doi:10.1038/299715a0.
Nesbitt, H. W., and G. M. Young (1984), Prediction of some weathering trends of plutonic and volcanic-rocks based on thermodynamic and kinetic considerations, *Geochim. Cosmochim. Acta*, *48*(7), 1523–1534, doi:10.1016/0016-7037(84)90408-3.
Nesbitt, H. W., and G. M. Young (1996), Petrogenesis of sediments in the absence of chemical weathering: Effects of abrasion and sorting on bulk composition and mineralogy, *Sedimentology*, *43*(2), 341–358, doi:10.1046/j.1365-3091.1996.d01-12.x.
Nesbitt, H. W., and R. E. Wilson (1992), Recent chemical weathering of basalts, *Am. J. Sci.*, *292*(10), 740–777.
Nesbitt, H. W., G. M. Young, S. M. McLennan, and R. R. Keays (1996), Effects of chemical weathering and sorting on the petrogenesis of siliciclastic sediments, with implications for provenance studies, *J. Geol.*, *104*(5), 525–542, doi:10.1086/629850.
Newsom, H. E., et al. (2016), The materials at an unconformity between the Murray and Stimson Formations at Marias Pass, Gale crater, Mars, presented at *47th Lunar and Planetary Science Conference*, Abstract 2397, LPI, Houston, Tex.
Nyquist, L. E., C.-Y. Shih, F. M. McCubbin, A. R. Santos, C. K. Shearer, Z. X. Peng, P. V. Burger, and C. B. Agee (2016), Rb-Sr and Sm-Nd isotopic and REE studies of igneous components in the bulk matrix domain of Martian breccia Northwest Africa 7034, *Meteorit. Planet. Sci.*, *51*(3), 483–498, doi:10.1111/maps.12606.
O'Connell-Cooper, C. D., et al. (2016), Preliminary comparison of soils within Gale crater to those from Gusev Crater and Meridiani Planum, presented at *47th Lunar and Planetary Science Conference*, Abstract 2477, LPI, Houston, Tex.
Ohta, T. (2004), Geochemistry of Jurassic to earliest Cretaceous deposits in the Nagato Basin, SW Japan: Implication of factor analysis to sorting effects and provenance signatures, *Sediment. Geol.*, *171*(1–4), 159–180, doi:10.1016/j.sedgeo.2004.05.014.
Palomares, M., and J. Arribas (1993), Modern stream sands from compound crystalline sources: Composition and sand generation index, in *Processes Controlling the Composition of Clastic Sediments*, *Geological Society of America Special Paper*, vol. 284, edited by M. J. Johnsson and A. Basu, pp. 313–322, Boulder, Colo.
Palucis, M. C., W. E. Dietrich, A. G. Hayes, R. M. E. Williams, S. Gupta, N. Mangold, H. Newsom, C. Hardgrove, F. Calef, and D. Y. Sumner (2014), The origin and evolution of the Peace Vallis fan system that drains to the Curiosity landing area, Gale crater, Mars, *J. Geophys. Res. Planets*, *119*, 705–728, doi:10.1002/2013JE004583.
Papike, J. J., J. M. Karner, C. K. Shearer, and P. V. Burger (2009), Silicate mineralogy of Martian meteorites, *Geochim. Cosmochim. Acta*, *73*(24), 7443–7485, doi:10.1016/j.gca.2009.09.008.
Press, W. H., S. A. Teukolsky, W. T. Vetterling, and B. P. Flannery (1992), *Numerical Recipes in FORTRAN: The Art of Scientific Computing*, 2nd ed., pp. 963, Cambridge Univ. Press, Cambridge.
Ragland, P. C. (1989), *Basic Analytical Petrology*, pp. 369, Oxford Univ. Press, Oxford.
Reid, M. J., A. J. Gancarz, and A. L. Albee (1973), Constrained least-squares analysis of petrologic problems with an application to lunar sample 12040, *Earth Planet. Sci. Lett.*, *17*(2), 433–445, doi:10.1016/0012-821x(73)90212-4.
Rieder, R., T. Economou, H. Wanke, A. Turkevich, J. Crisp, J. Bruckner, G. Dreibus, and H. Y. McSween (1997), The chemical composition of Martian soil and rocks returned by the mobile Alpha Particle X-ray Spectrometer: Preliminary results from the X-ray mode, *Science*, *278*, 1771.
Rieder, R., et al. (2004), Chemistry of rocks and soils at Meridiani Planum from the Alpha Particle X-ray Spectrometer, *Science*, *306*(5702), 1746–1749, doi:10.1126/science.1104358.
Rittmann, A. (1973), *Stable Mineral Assemblages of Igneous Rocks: A Method of Calculation*, pp. 262, Springer-Verlag, New York.
Roeder, P. (2006), Cotectic proportions of olivine and spinel in olivine-tholeiitic basalt and evaluation of pre-eruptive processes, *J. Petrol.*, *47*(5), 883–900, doi:10.1093/petrology/egi099.
Rogers, A. D., and H. Nekvasil (2015), Feldspathic rocks on Mars: Compositional constraints from infrared spectroscopy and possible formation mechanisms, *Geophys. Res. Lett.*, *42*, 2619–2626, doi:10.1002/2015GL063501.
Rubey, W. W. (1933), The size-distribution of heavy minerals within a water-laid sandstone, *J. Sediment. Petrol.*, *3*(1), 3–29.
Sack, R. O., D. Walker, and I. S. E. Carmichael (1987), Experimental petrology of alkaline lavas: constraints on cotectics of multiple saturation in natural basic magmas, *Contrib. Mineral. Petrol.*, *96*, 1–23.
Santos, A. R., C. B. Agee, F. M. McCubbin, C. K. Shearer, P. V. Burger, R. Tartèse, and M. Anand (2015), Petrology of igneous clasts in Northwest Africa 7034: Implications for the petrologic diversity of the Martian crust, *Geochim. Cosmochim. Acta*, *157*, 56–85, doi:10.1016/j.gca.2015.02.023.
Sautter, V., et al. (2015), In situ evidence for continental crust on early Mars, *Nat. Geosci.*, *8*(8), 605–609, doi:10.1038/ngeo2474.
Sautter, V., et al. (2016), Magmatic complexity on early Mars as seen through a combination of orbital, in-situ and meteorite data, *Lithos*, *254–255*, 36–52, doi:10.1016/j.lithos.2016.02.023.
Schieber, J., S. Gupta, J. Grotzinger, and R. Suarez-Rivera (2013), Hydraulic fracturing of Martian mudstones, presented at *Geological Society of America Annual Conference*, vol. 45, p. 39, Denver, Colo.

Schmidt, M. E., et al. (2014), Geochemical diversity in first rocks examined by the Curiosity rover in Gale crater: Evidence for and significance of an alkali and volatile-rich igneous source, *J. Geophys. Res. Planets*, *119*, 64–81, doi:10.1002/2013JE004481.
Shearer, C. K., P. V. Burger, J. J. Papike, L. E. Borg, A. J. Irving, and C. Herd (2008), Petrogenetic linkages among Martian basalts: Implications based on trace element chemistry of olivine, *Meteorit. Planet. Sci.*, *43*(7), 1241–1258.
Sheldon, N. D. (2003), Pedogenesis and geochemical alteration of the picture gorge subgroup, Columbia river basalt, Oregon, *Geol. Soc. Am. Bull.*, *115*(11), 1377–1387, doi:10.1130/B25223.1.
Siebach, K. L., and J. P. Grotzinger (2014), Characterizing sandstone porosity along Curiosity's traverse using MAHLI imagery, paper presented at Eighth International Conference on Mars, Pasadena, Calif., Abstract 1466.
Siebach, K. L., J. P. Grotzinger, L. C. Kah, K. M. Stack, M. Malin, R. Leveille, and D. Y. Sumner (2014), Subaqueous shrinkage cracks in the Sheepbed mudstone: Implications for early fluid diagenesis, Gale crater, Mars, *J. Geophys. Res. Planets*, *119*, 1597–1613, doi:10.1002/2014JE004623.
Slatt, R. M., and N. Eyles (1981), Petrology of glacial sand - implications for the origin and mechanical durability of lithic fragments, *Sedimentology*, *28*(2), 171–183, doi:10.1111/j.1365-3091.1981.tb01675.x.
Slingerland, R. L. (1977), The effects of entrainment on the hydraulic equivalence relationships of light and heavy minerals, *J. Sediment. Petrol.*, *47*, 753–770.
Smith, G. A., and J. E. Lotosky (1995), What factors control the composition of andesitic sand, *J. Sediment. Res.*, *A65*(1), 91–98.
Stack, K. M., et al. (2014), Diagenetic origin of nodules in the Sheepbed member, Yellowknife Bay formation, Gale crater, Mars, *J. Geophys. Res. Planets*, *119*, 1637–1664, doi:10.1002/2014JE004617.
Stolper, E. M., et al. (2013), The petrochemistry of Jake_M: A Martian mugearite, *Science*, *341*(6153), 1,239,463, doi:10.1126/science.1239463.
Szabó, T., G. Domokos, J. P. Grotzinger, and D. J. Jerolmack (2015), Reconstructing the transport history of pebbles on Mars, *Nat. Commun.*, *6*, 8366, doi:10.1038/ncomms9366.
Taylor, S. M., and S. M. McLennan (2009), *Planetary Crusts: Their Composition, Origin, and Evolution*, Cambridge Univ. Press, Cambridge, New York.
Thompson, L. M., et al. (2016), Potassium-rich sandstones within the Gale impact crater, Mars: The APXS perspective, *J. Geophys. Res. Planets*, *121*, 1981–2003, doi:10.1002/2016JE005055.
Thompson, L., M. Schmidt, G. Perrett, B. Elliott, R. Gellert, M. Fisk, and A. Team (2014), K-Rich Rocks at Gale, Dingo Gap to the Kimberley: An APXS perspective, presented at *Eighth International Conference on Mars*, Abstract 1433, Pasadena, Calif.
Thompson, L., R. Gellert, J. G. Spray, L. Kah, A. Team, and M. S. Team (2015), The composition of the basal Murray Formation at Pahrump Hills, Gale crater, Mars, presented at *46th Lunar and Planetary Science Conference*, Abstract 1429, LPI, Houston, Tex.
Treiman, A. H., and J. Filiberto (2015), Geochemical diversity of shergottite basalts: Mixing and fractionation, and their relation to Mars surface basalts, *Meteorit. Planet. Sci.*, *50*(4), 632–648, doi:10.1111/maps.12363.
Treiman, A. H., et al. (2016), Mineralogy, provenance, and diagenesis of a potassic basaltic sandstone on Mars: CheMin X-ray diffraction of the windjana sample (Kimberley area, Gale crater), *J. Geophys. Res. Planets*, *121*, 75–106, doi:10.1002/2015JE004932.
VanBommel, S. J., R. Gellert, J. A. Berger, J. L. Campbell, L. M. Thompson, K. S. Edgett, M. J. McBride, M. E. Minitti, I. Pradler, and N. I. Boyd (2016), Deconvolution of distinct lithology chemistry through oversampling with the Mars Science Laboratory Alpha Particle X-Ray Spectrometer, *X-Ray Spectrom.*, *45*(3), 155–161, doi:10.1002/xrs.2681.
Vaniman, D. T., D. L. Bish, S. J. Chipera, C. I. Fialips, J. W. Carey, and W. C. Feldman (2004), Magnesium sulphate salts and the history of water on Mars, *Nature*, *431*(7009), 663–665, doi:10.1038/nature02973.
Vaniman, D., et al. (2014), Mineralogy of a mudstone at Yellowknife Bay, Gale crater, Mars, *Science*, *343*(6169), doi:10.1126/science.1243480.
von Eynatten, H., R. Tolosana-Delgado, and V. Karius (2012), Sediment generation in modern glacial settings: Grain-size and source-rock control on sediment composition, *Sediment. Geol.*, *280*, 80–92, doi:10.1016/j.sedgeo.2012.03.008.
Walter, M. J., T. W. Sisson, and D. C. Presnall (1995), A mass proportion method for calculating melting reactions and application to melting of model upper-mantle lherzolite, *Earth Planet. Sci. Lett.*, *135*(1–4), 77–90, doi:10.1016/0012-821x(95)00148-6.
Weltje, G. J., and H. von Eynatten (2004), Quantitative provenance analysis of sediments: Review and outlook, *Sediment. Geol.*, *171*(1–4), 1–11, doi:10.1016/j.sedgeo.2004.05.007.
Wentworth, C. K. (1922), A scale of grade and class terms for clastic sediments, *J. Geol.*, *30*(5), 377–392.
Whetten, J. T., J. C. Kelley, and L. G. Hanson (1969), Characteristics of Columbia river sediment and sediment transport, *J. Sediment. Petrol.*, *39*(3), 1149–1166.
Whitmore, G. P., K. A. W. Crook, and D. P. Johnson (2004), Grain size control of mineralogy and geochemistry in modern river sediment, New Guinea collision, Papua New Guinea, *Sediment. Geol.*, *171*(1–4), 129–157, doi:10.1016/j.sedgeo.2004.03.011.
Wilkinson, J. F. G. (1967), The petrography of basaltic rocks, in *Basalts: The Poldervaart Treatise on Rocks of Basaltic Composition*, edited by H. H. Hess and A. Poldervaart, pp. 163–214, Interscience Publications, New York.
Williams, R. M., et al. (2013), Martian fluvial conglomerates at Gale crater, *Science*, *340*(6136), 1068–1072, doi:10.1126/science.1237317.
Wittmann, A., R. L. Korotev, B. L. Jolliff, A. J. Irving, D. E. Moser, I. Barker, and D. Rumble (2015), Petrography and composition of Martian regolith breccia meteorite Northwest Africa 7475, *Meteorit. Planet. Sci.*, *50*(2), 326–352, doi:10.1111/maps.12425.
Worden, R. H., and S. D. Burley (2003), Sandstone diagenesis: The evolution of sand to stone, in *Sandstone Diagenesis: Recent and Ancient*, edited by S. D. Burley and R. H. Worden, pp. 1–44, Blackwell Publishing Ltd., Oxford, U. K.
Yen, A. S., et al. (2006), Nickel on Mars: Constraints on meteoritic material at the surface, *J. Geophys. Res.*, *111*, E12S11, doi:10.1029/2006JE002797.
Yin, Q.-Z., et al. (2014), An Earth-like beginning for ancient Mars indicated by alkali-rich volcanism at 4.4 Ga, presented at *45th Lunar and Planetary Science Conference*, Abstract 1320, LPI, Houston, Tex.